CHARLES UNIVERSITY
Faculty of Science

Study programme: Analytical Chemistry

Mgr. Jan Rejšek

DEVELOPMENT AND APPLICATIONS OF AMBIENT MASS SPECTROMETRY TECHNIQUES

Vývoj a aplikace technik ambientní hmotnostní spektrometrie

Doctoral thesis

Supervisor: doc. RNDr. Josef Cvačka, Ph.D.

Prague 2017

Supervisor: doc. RNDr. Josef Cvačka, Ph.D.
Institute of Organic Chemistry and Biochemistry of the CAS

Supervisor-consultant: prof. RNDr. Pavel Coufal, Ph.D.
Faculty of Science, Charles University in Prague

Prohlášení

Prohlašuji, že jsem závěrečnou práci zpracoval samostatně a že jsem uvedl všechny použité informační zdroje a literaturu. Tato práce ani její podstatná část nebyla předložena k získání jiného nebo stejného akademického titulu.

V Praze, …… ……

Mgr. Jan Rejšek

PREFACE

Foremost, I would like to give thanks to my supervisor doc. Josef Cvačka, because his ideas and guidance have made this thesis a reality. I thank my colleagues from Mass Spectrometry Group, especially Dr. Vladimír Vrkoslav, for all their help. I would like to express my grateful thanks to the Development Workshops of IOCB, namely Ing. Vít Pokorný and Dr. Vladimír Přibyl, for their indispensable assistance on this project. Last but not least, I thank colleagues from Mass Spectrometry and Metabolomics Group (T. J. Kauppila group), University of Helsinki, for the fruitful cooperation.

This doctoral thesis includes results obtained during my Ph.D. studies from 2013 to 2017 at the Department of Analytical Chemistry, Faculty of Science, Charles University in Prague. The work was carried out in the laboratories of the Mass Spectrometry Group at the Institute of Organic Chemistry and Biochemistry of the Czech Academy of Sciences, Prague, and in the laboratories of the Division of Pharmaceutical Chemistry and Technology, Faculty of Pharmacy, University of Helsinki, Helsinki, Finland.

The work described in the doctoral thesis was financially supported by Charles University in Prague (project GAUK232515), Specific University Research (SVV Project, Charles University in Prague), RVO Project of the Czech Academy of Sciences 61388963, the Internal Support Program for Projects of International Collaboration of the Czech Academy of Sciences M200551204, the Czech Science Foundation (projects No. 13-25137P and No. P206/12/0750).

ABSTRACT (EN)

Ambient mass spectrometry defines the versatile group of methods providing analysis of solid sample surfaces and liquids in an open atmospheric pressure environment, where the sample is simultaneously accessible to another treatment. Ambient mass spectrometry is a sharply developing research area in the analytical chemistry. It provides fast, direct analysis of objects without any sample pretreatment with the use of the mass spectrometer. Desorption electrospray ionization (DESI) and desorption atmospheric pressure photoionization (DAPPI) equipped with software control of the sample holder were investigated in this doctoral thesis. These methods use a spray of solvents for desorption and ionization molecules from solid substrate and they are suitable tools for mass spectrometry imaging (MSI) of low molecular organic compounds, where the chemical identity of molecules present on a surface is examined as a function of spatial distribution.

This project deals with applications and instrumental development. As for the applications, the position of the defense glands on insect bodies, separation of the lipids in complex mixtures on thin-layer chromatography (TLC) plates, or steroid metabolites in woman urine during pregnancy were thus investigated. As for the instrumental development, the most important point is the construction of a new ion source for ambient mass spectrometry imaging of nonplanar samples. A visible trend interwoven with the project is a progress from the planar to the nonplanar sample analysis.

KEYWORDS (EN)

ambient mass spectrometry techniques; desorption atmospheric pressure photoionization; desorption electrospray ionization; mass spectrometry imaging; insect chemical defense; exocrine glands; termite; stink bug; thin-layer chromatography; lipids; vernix caseosa; pregnancy; laser triangulation

ABSTRAKT (CZ)

Ambientní hmotnostní spektrometrie zahrnuje širokou skupinu metod umožňujících analýzu povrchu tuhých látek a kapalin v otevřeném prostoru vně hmotnostního spektrometru, kdy je vzorek přístupný k vnějšímu zásahu i během analýzy. Ambientní hmotnostní spektrometrie je dynamicky se rozvíjející oblastí analytické chemie. Umožňuje rychlou přímou analýzu objektů vně přístroje bez předchozí úpravy vzorku. V této práci byla studována desorpční ionizace elektrosprejem (DESI) a desorpční fotoionizace za atmosférického tlaku (DAPPI) se softwarově ovládanou polohou držáku vzorku. Tyto metody využívají sprejování rozpouštědel k desorpci a ionizaci analytu z pevného substrátu a jsou vhodné pro zobrazovací hmotnostní spektrometrii nízkomolekulárních organických sloučenin, kde je chemická identita molekul na povrchu analyzovaného objektu zkoumána jako funkce prostorové distribuce.

Tento projekt se zabývá aplikacemi a instrumentálním vývojem. Pokud jde o aplikace, byla studována poloha hmyzích obranných žláz, separace lipidů v reálných vzorcích pomocí tenkovrstvé chromatografie (TLC), nebo metabolity steroidů v ženské moči v průběhu těhotenství. Ohledně instrumentálního vývoje, nejdůležitějším bodem byla konstrukce nového iontového zdroje pro ambientní zobrazovací hmotnostní spektrometrii neplanárních objektů. Zřetelný trend spjatý s celým projektem je postup od analýzy planárních povrchů k neplanárním.

KLÍČOVÁ SLOVA (CZ)

techniky ambientní hmotnostní spektrometrie; desorpční fotoionizace za atmosférického tlaku; desorpční ionizace elektrosprejem; zobrazovací hmotnostní spektrometrie; chemická obrana hmyzu; exokrinní žlázy; termit; ploštice; tenkovrstvá chromatografie; lipidy; vernix caseosa; těhotenství; laserová triangulace

CONTENTS

LIST OF ORIGINAL PUBLICATIONS

This doctoral thesis is based on the following publications:

I Jan Rejšek, Vladimír Vrkoslav, Robert Hanus, Anu Vaikkinen, Markus Haapala, Tiina J. Kauppila, Risto Kostiainen, Josef Cvačka, The detection and mapping of the spatial distribution of insect defense compounds by desorption atmospheric pressure photoionization Orbitrap mass spectrometry, *Analytica Chimica Acta* **2015**, *886*, 91–97.

II Jan Rejšek, Vladimír Vrkoslav, Anu Vaikkinen, Markus Haapala, Tiina J. Kauppila, Risto Kostiainen, Josef Cvačka, Thin-layer chromatography/desorption atmospheric pressure photoionization Orbitrap mass spectrometry of lipids, *Analytical Chemistry* **2016**, *88*, 12279–12286.

III Jan Rejšek, Vladimír Vrkoslav, Vít Pokorný, Vladimír Přibyl, Josef Cvačka, Ion source with laser triangulation for ambient mass spectrometry of nonplanar samples, *Analytical Chemistry*, Just Accepted Manuscript.

IV Anu Vaikkinen, Jan Rejšek, Vladimír Vrkoslav, Tiina J. Kauppila, Josef Cvačka, Risto Kostiainen, Feasibility of desorption atmospheric pressure photoionization and desorption electrospray ionization mass spectrometry to urinary steroid metabolites during pregnancy, *Analytica Chimica Acta* **2015**, *880*, 84–92.

The publications are referred in the text by their Roman numerals.

DECLARATION OF AUTHORSHIP

As a representative of the co-authors, I declare that Mgr. Jan Rejšek participated in the publications listed below:

I The experimental work was carried out by the author. The manuscript was written by the author with contributions from others.

(participation 80 %)

II The experimental work was carried out by the author. The manuscript was written by the author with contributions from others.

(participation 80 %)

III The experimental work was carried out by the author. The manuscript was written by the author with contributions from others. The ion source was constructed by Vít Pokorný and Vladimír Přibyl.

(participation 80 %)

IV The author partly cooperated on the experimental work during his three months' stay in Finland.

(participation 20 %)

……..……...……

doc. RNDr. Josef Cvačka, Ph.D.

ABBREVIATIONS AND SYMBOLS

AP-MALDI	atmospheric pressure matrix-assisted laser desorption/ionization
APCI	atmospheric pressure chemical ionization
API	atmospheric pressure ionization
APPI	atmospheric pressure photoionization
CI	chemical ionization
CID	collision-induced dissociation
DAPCI	desorption atmospheric pressure chemical ionization
DAPPI	desorption atmospheric pressure photoionization
DART	direct analysis in real time
DBDI	dielectric barrier discharge ionization
DESI	desorption electrospray ionization
DHEA	dehydroepiandrosterone
DI	desorption/ionization
EA	electron affinity
EASI	easy ambient sonic-spray ionization
ECN	equivalent carbon number
EESI	extractive electrospray ionization
EI	electron ionization
ELDI	electrospray-assisted laser desorption ionization
ESI	electrospray ionization
FA-APGDI	flowing afterglow-atmospheric pressure glow discharge
fp	frontal pore
GC	gas chromatography
GDI	glow discharge ionization
HPTLC	high-performance thin-layer chromatography
HRMS	high resolution mass spectrometry

I	intensity
IE	ionization energy
IR-LADESI	infrared laser-assisted desorption electrospray ionization
IS	internal standard
LAESI	laser-assisted electrospray ionization
LC	liquid chromatography
LDI	laser desorption/ionization
LLE	liquid–liquid-extraction
LOD	limit of detection
LTP	low-temperature plasma ionization
m/z	mass-to-charge ratio
MALDESI	matrix-assisted laser desorption electrospray ionization
MALDI	matrix-assisted laser desorption/ionization
MS	mass spectrometry
MS^2	tandem mass spectrometry
MSI	mass spectrometry imaging
ND-EESI	neutral desorption EESI
NP	normal-phase
p	probability value
PA	proton affinity
PADI	plasma-assisted desorption/ionization
PI	photoionization
PMMA	polymethylmethacrylate
PSI	paper-spray ionization
PTFE	polytetrafluoroethylene
QqQ	triple quadrupole
r	reservoir
RP	reversed-phase
RSD	relative standard deviation
R_f	retardation factor

R_S	chromatographic resolution
SPE	solid phase extraction
SSI	sonic-spray ionization
T	testosterone
TG	triacylglycerol
TLC	thin-layer chromatography
TRIAC	triode for alternating current
WE	wax ester

1 INTRODUCTION

Mass spectrometry (MS) is an instrumental versatile analytical technique characterized by high speed, sensitivity, and selectivity. The mass spectrometer consists of three basic parts: (1) Ion source that generates ions in the gas phase; (2) Mass analyzer that uses various physical and chemical effects (e.g. a trajectory of charged particles in electromagnetic field or time of flight of ions) to separate ions; (3) Ion detector. The selection of the ion source is critical in determining the kinds of compounds that will be detected, as well as the sample types that can be analyzed.

To deal with a great variety of atoms and molecules, and matrices and mixtures, MS needs to promote efficient ionization to generate ions, ideally, for each component that can be transferred to the high vacuum environment of mass spectrometers where they are characterized and counted. Traditional MS ionization techniques, such as electron ionization (EI), or chemical ionization (CI) were performed on gaseous molecules. Thermally unstable and less volatile molecules were thus simply untreatable. In the 1980s, Fenn and co-workers showed that electrospray ionization (ESI) at atmospheric pressure can be combined with mass spectrometry[1] to enable the study of large biomolecules. ESI launched a revolutionary concept of MS ionization in which ions were produced directly from molecules present and pre-ionized in solutions, typically via protonation, deprotonation, cationization or anionization. These solvated ions are then "ejected" by electro-spraying directly from the analyte solution initially into the atmospheric pressure gas phase. Finally, the relatively cold gaseous ions (most frequently little or no dissociation occurs during ESI), most typically $[M + H]^+$, $[M - H]^-$, and $[M + Na]^+$ species, are subsequently conducted from the ambient atmosphere into the high vacuum of the mass spectrometer for counting and characterization. ESI and a range of related atmospheric pressure ionization (API) techniques, for example, atmospheric pressure chemical ionization (APCI), atmospheric pressure photoionization (APPI),[2,3] and atmospheric pressure matrix-assisted laser desorption/ionization (AP-MALDI)[4] have tremendously broadened the scope of MS analysis. Examples of such new abilities are provided, for instance, by the ionization and mass measurements of proteins, viruses,[5] and even intact bacteria. Although ESI and other API techniques enhanced MS analysis,

they still required a substantial amount of sample pretreatment such as extraction and dissolution, which may cause chemical interferences and may disturb natural analyte spatial distribution in the matrix.

The introduction of desorption electrospray ionization (DESI) by Cooks and co-workers in 2004[6] triggered the deep interest and the huge development in a new family of direct sampling desorption/ionization (DI) techniques, known collectively as ambient mass spectrometry. These techniques have shown that MS can handle molecules directly in their natural environments or when placed on auxiliary surfaces. Desorption/ionization techniques were forming the required gaseous ions under ambient open-atmosphere conditions with very little or no sample preparation.

These revolutionary desorption/ionization techniques have the compelling advantages of simplicity. As a result of the elimination of time-consuming and sometimes chemically disturbing sample preparation steps, they enable straightforward MS analysis. The simplicity has increased the speed of MS by delivering ease of use and, naturally, less training and specialization requirements for the analyst.

This work deals with applications and development of two ambient ionization techniques, namely desorption atmospheric pressure photoionization (DAPPI)[7] and DESI.[6]

1.1 AMBIENT MASS SPECTROMETRY TECHNIQUES

Apart from other ionization techniques used in mass spectrometry, ambient techniques[8] meet the following criteria: (1) they enable the direct analysis without the sample pretreatment, such as pre-concentration, extraction, derivatization, dissolution, chromatographic or electrophoretic separation; (2) they are compatible with all types of mass spectrometers regardless of the mass analyzer used; (3) they are soft ionization techniques, i.e., the generated ions have similar inner energy like in API techniques (ESI, APCI, APPI etc.).

Ambient mass spectrometry techniques allow analyzing living organisms such as insects in real time, e.g., to monitor released defensive secretion caused by the outer intervention. These studies are very helpful in chemical ecology. Chemical ecology is a

discipline that investigates insect behavior (mating, defensive[9] etc.) mediated by chemical compounds. Ambient techniques also enable, among other things, rapid monitoring of metabolome or coupling with thin-layer chromatography.[10] Recently, the possibility of nonplanar surface analysis is being thoroughly examined.[11]

The majority of ambient techniques uses the principle of desorption/ionization. They allow rapid, selective, sensitive, qualitative and quantitative chemical and biochemical analysis in combination with easy use. Nowadays, we recognize over 30 of these techniques. Table 1.1 summarizes the chronological (the first publication) list of the most widespread techniques.

Table 1.1. The list of the most common techniques in ambient mass spectrometry.

Acronym	Description	Year	Reference
DESI	desorption electrospray ionization	2004	ref. 6
DART	direct analysis in real time	2005	ref. 12
ASAP	atmospheric solids analysis probe	2005	ref. 13
DAPCI	desorption atmospheric pressure chemical ionization	2006	ref. 14
EASI	easy ambient sonic-spray ionization	2006	ref. 15
EESI	extractive electrospray ionization	2006	ref. 16
ELDI	electrospray-assisted laser desorption ionization	2006	ref. 17
MALDESI	matrix-assisted laser desorption electrospray ionization	2006	ref. 18
ND-EESI	neutral desorption EESI	2007	ref. 19
DAPPI	desorption atmospheric pressure photon ionization	2007	ref. 7
PADI	plasma-assisted desorption/ionization	2007	ref. 20
DBDI	dielectric barrier discharge ionization	2007	ref. 21
LAESI	laser-assisted ESI	2007	ref. 22
FA-APGDI	flowing afterglow-atmospheric pressure glow discharge	2008	ref. 23
IR-LADESI	infrared laser-assisted desorption ESI	2008	ref. 24
LTP	low-temperature plasma ionization	2008	ref. 25
PSI	paper spray ionization	2010	ref. 26

At present, there is no unified classification of ambient techniques. For this reason, they could be divided according to the various criteria. Table 1.2 shows three main modes of ambient ionization methods.[27]

Table 1.2. Three main modes of ambient ionization methods.[27]

	Ionization	State of the sample	Examples
spray-based	momentum desorption–solvent extraction–ionization/direct ionization	solid and liquid	DESI
plasma-based	thermal desorption–ionization	solid, liquid and gas	DART
laser-based	laser ablation–electrospray extraction–ionization	solid and liquid	ELDI

Another way of ambient technique classification done based on the different ionization mechanisms is outlined in Figure 1.1.[28]

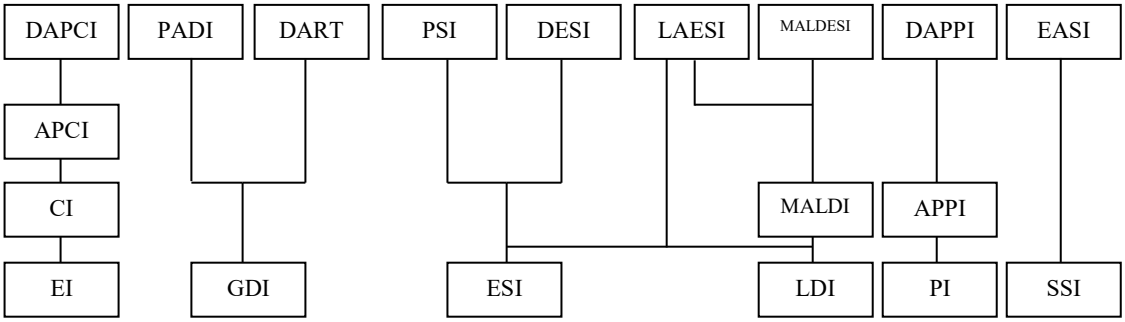

Figure 1.1. Ambient technique classification according to the different ionization mechanisms. GDI, glow discharge ionization; LDI, laser desorption/ionization; MALDI, matrix-assisted laser desorption/ionization; PI, photoionization; PSI, paper-spray ionization; SSI, sonic-spray ionization.[28]

1.2 DESORPTION ATMOSPHERIC PRESSURE PHOTOIONIZATION

Desorption atmospheric pressure photoionization (DAPPI) is an ambient ionization technique introduced in 2007.[7] A key part of the DAPPI instrumentation is an electrically heated nebulizer microchip, which is used as a source of hot confined jet of solvent vapour and nebulizing gas.[29] Acetone and toluene are the most frequently used solvents, which take part in the photoionization due to the ion-molecule reactions in the gas phase.[30] The mechanism of desorption in DAPPI is thermal, while the ionization is initiated by photons emitted from a vacuum ultraviolet lamp. A krypton lamp producing highly energetic 10 eV and 10.6 eV (123.9 nm and 116.9 nm) UV photons is positioned to illuminate the analyzed area. Thanks to the photoionization, the DAPPI method covers a broad range of

analytes including nonpolar compounds that are difficult to ionize by most ambient ionization techniques.

1.2.1 Mechanism

The mechanism of desorption and ionization is a combination of thermal and chemical processes. A hot mixture of solvent vapor and nebulizing gas is directed on the sample that is irradiated by the ultraviolet lamp. Since the increasing temperature of the jet leads to the rise in a signal intensity, the desorption is bound to be thermal. In addition, the solubility of analyzed molecules in solvents also undoubtedly affects the desorption. The ionization is similar to APPI.[31] It is a photoionization in the presence of dopant (solvent such as acetone, toluene, or anisole) with ion-molecule reactions in the gas phase.[30] Photons emitted by the UV lamp activate the process of ionization by creating charged solvent molecules and thermal electrons (Equation 1.1).

$$S + h\nu \longrightarrow S^{+\bullet} + e^{-} \qquad (1.1)$$

Then, the ion-molecule reactions in the gas phase similar to APPI carry out, for example:[30,32]

$$S^{+\bullet} + M \longrightarrow S + M^{+\bullet}, \text{ if } IE(M) < IE(S) \qquad (1.2)$$

$$S^{+\bullet} + M \longrightarrow [S - H]^{\bullet} + [M + H]^{+}, \text{ if } PA(M) > PA(S) \qquad (1.3)$$

$$O_2 + e^{-} \longrightarrow O_2^{-\bullet} \qquad (1.4)$$

$$M + O_2^{-\bullet} \longrightarrow M^{-\bullet} + O_2, \text{ if } EA(M) > EA(O_2) \qquad (1.5)$$

$$M + e^{-} \longrightarrow M^{-\bullet}, \text{ if } EA(M) > 0 \text{ eV} \qquad (1.6)$$

$$M + O_2^{-\bullet} \longrightarrow [M - H + O]^{-} + OH^{\bullet} \qquad (1.7)$$

In course of the ionization in the positive mode, the molecules are ionized either by the proton transfer, if the proton affinity (PA) of the analyte is higher than of the interacted ion, or the charge exchange, if the ionization energy (IE) of the analyte is lower than of the interacted ion.[32] It is thus possible to ionize molecules with low PA by the

charge exchange, if they have IE low enough. Typical ions are then $[M + H]^+$, $M^{+\bullet}$ and $[M – H]^+$.

In course of the ionization in the negative mode, the molecules are ionized by the proton transfer, if the dissociation constant of the analyte in the gas phase is higher than of the interacted ion, or the electron capture, or the charge exchange, if the electron affinity (EA) of the analyte is higher than of the interacted ion.[32] Thermal electrons produced during the photoionization are captured by compounds with positive value of EA. Oxygen, which has EA 0.45 eV, is always present in the ion source and creates superoxide anion $O_2^{-\bullet}$ that can successively ionize analyte molecules. Typical ions are then $[M – H]^-$ and $M^{-\bullet}$.

Products of oxidation associated with the addition of one, or more oxygen atoms are often observed in mass spectra. The oxidation is caused by particles such as reactive neutral radicals, atomic oxygen, or hydroxyl radical, which are produced by the photolysis of O_2 and H_2O present in the atmosphere.[33]

1.2.2 Experimental conditions and instrumentation

Microchip. The type and the way of microchip manufacturing significantly influence the measurement. The nebulizer microchip consists of two glass plates bonded together. A liquid inlet channel, nebulizer gas inlet, vaporizer channel, and nozzle are etched on the top plate, and a platinum heater is integrated on the blank bottom plate. Liquid entering the chip through a silica capillary is mixed with nebulizer gas in the heated vaporizer. The nozzle creates a confined jet of the heated vapor as the vapor exits the chip.

Geometrical arrangement. The geometrical arrangement, which includes the positions of the microchip, the sample, the MS inlet capillary and the Krypton UV lamp (Figure 1.2), is seminal for DAPPI. It can be described by parameters angle of incidence α, the angle between MS inlet capillary and the sample β, the distance between the microchip and the sample d_1, the distance between the MS inlet capillary and the sample d_2, and the distance between the microchip and the MS inlet capillary d_3.

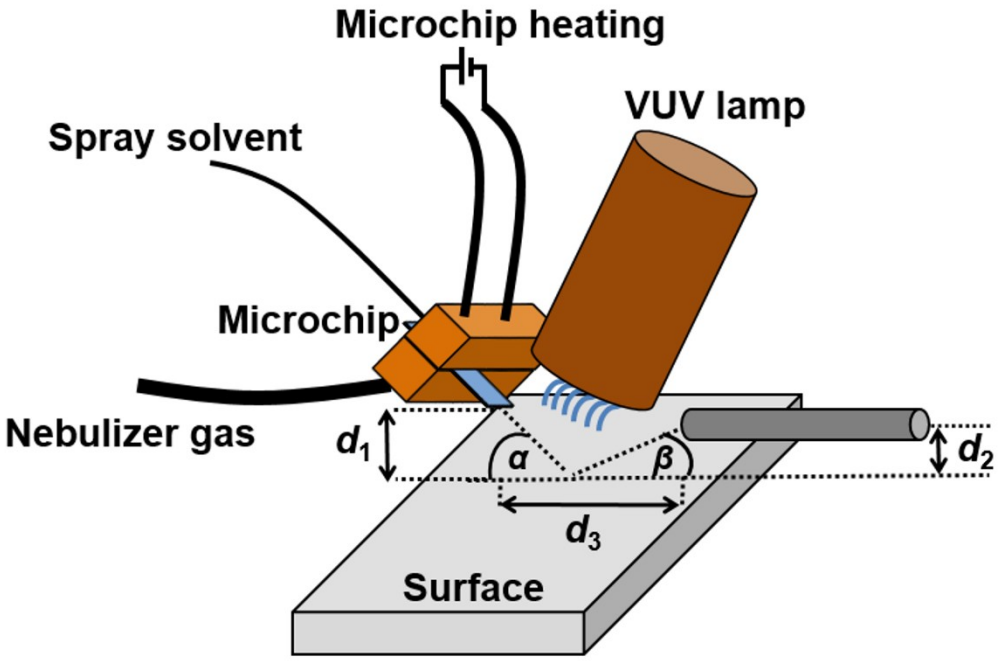

Figure 1.2. Scheme of the DAPPI-MS setup. α: angle of incidence. β: angle of reflection. d_1: microchip-to-surface distance. d_2: MS inlet capillary-to-surface distance. d_3: microchip-to-MS inlet capillary distance.

A hot jet of solvent vapor and nebulizing gas. In comparison with DESI, a relatively low flow rate of nebulizing gas (e.g. 180 ml·min^{-1}) is used. It results in a more narrow jet that ensures a well-localized and smaller spray plume. The speed of ejected jet at the nozzle is about 30 m·s^{-1},[7] whereas it is about 120 m·s^{-1} for DESI.[34] Lower kinetic energy of DAPPI jet in comparison to DESI do not downsize the desorption efficiency as it is driven thermally.

It was reported that further rise of solvent flow rate over 8 µl·min^{-1} do not cause a further rise in the ionization efficiency.[7] This phenomenon can be explained by the fact that certain amount of the dopant is necessary for the efficient ionization, but its overdose does not have any beneficial effect.

The use of an electric platinum heater allows rapid temperature adjustment. The emitted jet could be heated up to 350 ºC, being restricted by the thermal resistivity of the platinum heating element. The higher the temperature is applied, the higher the signal intensity is. The higher the analyte boiling point is, the higher the temperature should be employed.

Chemical conditions. The selection of solvent has an impact on the method selectivity and the ionization process.[32] As for the positive ion mode, anisole and toluene boost the creation of $M^{+\bullet}$, and they are thus suitable for the analysis of nonpolar compounds. Anisole and toluene have low IE. Therefore, they readily form cation radicals, which subsequently undergo the charge exchange with analyte molecules. Whereas acetone, hexane, propan-2-ol, and methanol enhance the creation of $[M + H]^+$, and they are thus the right choice for the analysis of polar compounds. In this case, the ionization carries out via the proton transfer. As for the negative ion mode, the examined solvents affected the signal intensity of studied ions but not their type.[32]

Sample surface. The type of sample surface (glass, paper, polymer, biological tissue etc.) has a dramatic effect on the signal intensity. It was reported that the best characteristics for DAPPI analysis have polymer materials such as polymethylmethacrylate (PMMA) and polytetrafluoroethylene (PTFE) owing to their low thermal conductivity, which brings on more efficient heating of the sampled spot.[32] Glass and paper provide sufficient response only in the positive ion mode. Surface material is likely not to affect the ionization process but the desorption efficiency, which is strongly dependent on the morphology and the microstructure of the material.

1.2.3 Applications

DAPPI has been used for numerous applications, among which are the detection of fatty acids, triacylglycerols, vitamins, sterols, and phospholipids from fish oil capsules, multivitamin tablets, and cow milk, then in the analyses of pesticides,[35] polyaromatic hydrocarbons,[35] street market confiscated drugs[36] and cannabis samples.[37] DAPPI has also been applied for MSI of parched leaves of Salvia.[38] The spatial distribution of small molecules like tocopherol and carnosol was visualized using high-resolution mass spectrometry with lateral resolution of about 1000 μm.

1.3 DESORPTION ELECTROSPRAY IONIZATION

DESI[6] is certainly the most common ambient ionization technique, which has been already applied for the countless samples. The analytes can be studied from their

biological matrix (e.g. skin, brain), or they can be placed on supporting surface (e.g. glass, paper, metal, TLC). It is a universal technique allowing the analysis of a broad range of molecules. Fundamental analytical figures of merit are strongly dependent on the analyte structure. Limit of detection for small molecules was published 1 to 10 fmol and the reproducibility of quantitative data was 5–10 %.[39]

1.3.1 Mechanism

A spray of fine charged droplets of the solvent from an electrospray impacts on the sample. The average droplet velocity is about 120 m s^{-1} and the average diameter of the droplet is about 3 μm.[34] The desorption carries out via so called "droplet pick-up" mechanism,[40] when the initial wetting of the surface (to form a thin film) by the solvent to dissolve the analyte occurs, followed by splashing on the arrival of droplets with emission of secondary microdroplets. These microdroplets are then ionized by ESI mechanism and they are transported to the mass spectrometer. The simulations of the DESI process show the formation of dozens of microdroplets resulting from a single droplet–thin film collision event.[41]

1.3.2 Experimental conditions and instrumentation

Geometrical arrangement. The geometrical arrangement, which includes the positions of the sprayer, the sample and the MS inlet capillary (Figure 1.3), is seminal for DESI. It can be described by parameters like the angle of incidence α, the angle between MS inlet capillary and the sample β, the distance between the sprayer and the sample d_1, the distance between the MS inlet capillary and the sample d_2, and the distance between the sprayer and the MS inlet capillary d_3.

The efficiency of DESI depends on the desorption of analyte from the surface, its transport to the mass spectrometer, and the ionization. Parameters α and d_1 affect directly the ionization, whereas parameters β and d_2 usually the sensitivity.

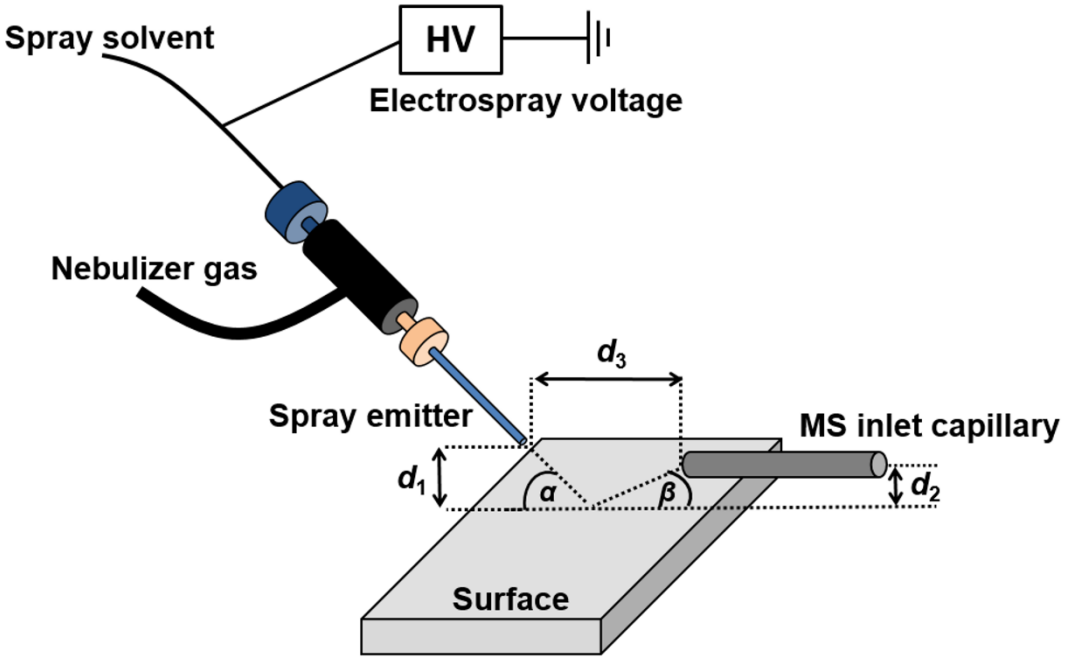

Figure 1.3. Scheme of the DESI-MS setup. α: angle of incidence. β: angle of reflection. d_1: sprayer-to-surface distance. d_2: MS inlet capillary-to-surface distance. d_3: sprayer-to-MS inlet capillary distance.

Spraying conditions. The spraying conditions (the flow rate of solvent and nebulizing gas, and the solvent capillary voltage) define size, charge, and speed of the formed droplets. The higher flow rate of the nebulizing gas reduces the droplet size but increases their speed. To a certain degree, this phenomenon is beneficial (as it supports desolvation), but the excessive value of the gas flow rate could result in an early evaporation, which lowers DESI efficiency.[42] Higher flow rate of the solvent brings about forming bigger droplets. In the extreme, solvent might excessively accumulate on the surface.

Chemical conditions. Similarly to ESI, the composition of spray solvent should be modified with respect to the analyte. The most common solvents are methanol, water, acetonitrile and their combinations. The most common additives are formic acid, ammonia, or ammonium acetate.

Sample surface. The type of sample surface (glass, paper, polymer, biological tissue etc.) has a dramatic effect on the signal intensity. The electric conductivity of the surface influences the ionization.[43] DESI mechanism involves forming of charged droplets, which is why the electric insulators are exclusively used. Electrostatic properties of the surface

are very important and affect, e.g., the signal stability. A significant characteristic is also the affinity of the analyte to the surface. The bigger the affinity is, the smaller the DESI efficiency is, owing to hampering of desorption. On account of this, the polymer materials, such as Teflon or Plexiglas, are beneficially used.

1.3.3 Applications

DESI has been already applied for the fast analysis of pharmaceutical products,[44] explosives,[45] biological imaging,[46] forensic imaging of inks[47] and counterfeits,[48] drugs in complex biological matrixes,[49] textile,[50] peptides[51] and proteins,[42] in proteomics,[52] metabolomics[53] and thin-layer chromatography.[54] It was also used for the analysis of plants,[55] natural products,[56] microorganisms *in vivo*,[57] monitoring of environment[58] and polymers.[59]

2 AIMS OF THE WORK

The overall aim of the work was an instrumental development and applications of DAPPI and DESI for surface analysis.

Specifically, the aims of the research were to develop:

- a rapid analytical technique which would make it possible to localize secretory gland openings on the insect body surface and characterize the compounds of the secretion using DAPPI-MS (I);
- a direct analytical technique for the detection of lipids separated on TLC plates by DAPPI-MS (II);
- a cost-effective technique for nonplanar surface analysis (III);
- a screening analytical technique to monitor urinary steroid metabolites during pregnancy (IV).

3 EXPERIMENTAL

This section briefly describes the materials, instrumentation, and ion source setups of the study. Details are provided in the original publications (I–IV).

3.1 CHEMICALS, MATERIALS, AND SAMPLES

The chemicals that were used are listed in Table 3.1 and the samples that were analyzed in Table 3.2.

Table 3.1. Chemicals used in the study.

Chemical	Manufacturer/supplier	Note	Publication
(*E*)-1-nitropentadec-1-ene	synthesized[60]	standard	I
(*E*)-dec-2-enal	Sigma-Aldrich, St. Louis, MO, USA	standard	I
(*E*)-hex-2-enal	Sigma-Aldrich, St. Louis, MO, USA	standard	I
(*E*)-oct-2-enal	Sigma-Aldrich, St. Louis, MO, USA	standard	I
(*E*)-undec-2-enal	Sigma-Aldrich, St. Louis, MO, USA	standard	I
(*E*,*E*)-deca-2,4-dienal	Sigma-Aldrich, St. Louis, MO, USA	standard	I
1,2-dioleoyl-hexadecane-1,2-diol	synthesized[61]	standard	II
1,3-dipalmitoyl-2-oleoyl-glycerol	Sigma-Aldrich, St. Louis, MO, USA	standard	II
2,3-oxidosqualene	Sigma-Aldrich, St. Louis, MO, USA	standard	II
2,5-dimethoxybenzoic acid	Sigma-Aldrich, St. Louis, MO, USA	standard	III
D_3-testosterone	Sigma-Aldrich, St. Louis, MO, USA	standard	IV

DHEA sulfate	Sigma-Aldrich, St. Louis, MO, USA	standard	IV
acetic acid	Lach-Ner, Neratovice, Czech Republic	modifier	II
	Sigma-Aldrich, St. Louis, MO, USA	modifier	IV
acetone	Sigma-Aldrich, St. Louis, MO, USA	solvent	I–IV
acetonitrile	Sigma-Aldrich, St. Louis, MO, USA	solvent	II
ammonium acetate	Sigma-Aldrich, St. Louis, MO, USA	modifier	IV
ammonium formate	Fluka Chemie GmbH, Buchs, Switzerland	modifier	II
ammonium hydroxide	Sigma-Aldrich, St. Louis, MO, USA	modifier	IV
androsterone glucuronide	Sigma-Aldrich, St. Louis, MO, USA	standard	IV
caffeine	Sigma-Aldrich, St. Louis, MO, USA	standard	III
chloroform	Penta, Chrudim, Czech Republic	solvent	II
cholesterol	Sigma-Aldrich, St. Louis, MO, USA	standard	II
cholesteryl oleate	Sigma-Aldrich, St. Louis, MO, USA	standard	II
citric acid	Lachema, Brno, Czech Republic	standard	III
diethyl ether	Penta, Chrudim, Czech Republic	solvent	II
	Sigma-Aldrich, St. Louis, MO, USA	solvent	IV
hexane	Sigma-Aldrich, St. Louis, MO, USA	solvent	II
linoleic acid	Nu-Chek-Prep, Elysian, MN, USA	standard	III
methanol	Sigma-Aldrich, St. Louis, MO, USA	solvent	I–IV

nitrogen	Messer, Bad Soden, Germany	nebulizer gas	I–IV
palmityl oleate	Sigma-Aldrich, St. Louis, MO, USA	standard	II
paracetamol	Sigma-Aldrich, St. Louis, MO, USA	standard	III
potassium acetate	Mallinckrodt Baker B.V., Deventer, The Netherlands	modifier	IV
potassium carbonate	Mallinckrodt Baker B.V., Deventer, The Netherlands	modifier	IV
pregnenolone-20,21-$^{13}C_2$-16,16-D_2 sulfate sodium salt	Sigma-Aldrich, St. Louis, MO, USA	standard	IV
sodium bicarbonate	VWR international, Espoo, Finland	modifier	IV
squalene	Sigma-Aldrich, St. Louis, MO, USA	standard	II
sulfuric acid	Lach-Ner, Neratovice, Czech Republic	visualizing agent	II
testosterone glucuronide	Sigma-Aldrich, St. Louis, MO, USA	standard	IV
thiabendazole	Sigma-Aldrich, St. Louis, MO, USA	standard	III
type HP-2 β-glucuronidase from *Helix pomatia*	Sigma-Aldrich, St. Louis, MO, USA	standard	IV
verapamil hydrochloride	Sigma-Aldrich, St. Louis, MO, USA	standard	I, II
water (Milli-Q)	Millipore, Molsheim, France	solvent	IV

The spray solvent for DAPPI was acetone (I, III, IV), or acetone/chloroform/10 mM ammonium formate in acetone–water (75:25:1; v/v/v) (II). The spray solvent for DESI was methanol (III), or methanol/water (1:1; v/v) + 0.1% ammonium hydroxide (IV). Stock solutions of the standards were prepared in methanol (I, III, IV), or chloroform (II). In APPI-MS (II) mobile phase composed of acetone/chloroform/10 mM ammonium formate in acetone−water (75:25:1; v/v/v) was used. In DAPPI, and DESI working solutions were sampled: (i) as a liquid droplet and

analysed from a PTFE film (I–IV), and TLC plate (II), or (ii) as a uniform coating and analysed from acrylic sheet (I), and photopolymer resin plastic object (III).

Table 3.2. Samples analyzed in the study and sample preparation methods employed.

Sample	Supplier/source	Sample preparation	Publication
termite soldier *Prorhinotermes simplex*	a mature laboratory colony at IOCB AS CR	Body extracts – immersing the specimens in acetone for 15 min.	I
		Frontal gland secretion – collected at the cervical section from the decapitated specimen.	
		Specimens – fixed on the glass slides, the dorsal body surface was examined.	
adult stink bug *Graphosoma lineatum*	collected near Prague, Czech Republic	Body extracts – immersing the specimens in acetone for 15 min.	I
		Specimens – fixed on the glass slides, the ventral body surface was examined.	
engraved acrylic sheets	acrylic sheets from Perspex, Blackburn, Great Britain	Acrylic sheets were modified by engraving regularly spaced channels.	I
thin-layer chromatography	plates from Merck KGaA, Darmstadt, Germany	The sample solutions (0.5 μL) were applied by Nanomat 4 on the starting line of the TLC plate, and the solvent was left to evaporate at room temperature. The TLC plate was then preconditioned for about 10 min in the Twin Trough chamber and developed using a linear (ascending) technique.	II
	Nanomat 4 from CAMAG, Muttenz, Switzerland		
	Twin Trough chamber from CAMAG, Muttenz, Switzerland		
vernix caseosa	volunteer	Total lipid extract was dissolved in chloroform.	II
urine	volunteer	DESI – prepared by SPE.[62]	IV
		DAPPI – hydrolyzed and prepared by LLE.[63,64]	
plastic objects	Deep Black photopolymer resin from Fun To Do,	Printed out by a 3D printer and uniformly coated with 2,5-dimethoxybenzoic acid.	III

	Alkmaar, The Netherlands		
coffee bean	local supermarket	Fixed on a glass slide pre-coated with a black non-transparent tape using a double-sided adhesive tape.	III
Smartie	local supermarket		III
chewing gum	local supermarket		III
Paramegal tablet	local pharmacy		III
mandarin orange	local supermarket		III
onion	local supermarket		III

3.2 INSTRUMENTATION

Table 3.3 lists the most relevant commercial instruments used in the work; the notes indicate their use. The in-house built heater of the protruded MS inlet capillary extension powered by a power supply based on TRIAC regulator of voltage was also employed.

Table 3.3. Commercial instruments used in the work.

Instrument/equipment	Manufacturer/supplier	Note	Publication
LTQ Orbitrap XL mass spectrometer	Thermo Fisher Scientific, San Jose, CA, USA	mass analysis	I–IV
6410 triple quadrupole MS	Agilent Technologies, Santa Clara, USA	mass analysis	IV
laser engraver 8015 Rayjet 50	Trotec Laser GmbH, Marchtrenk, Austria	engraving	I
TOS FN 20 milling machine	TOS, Čelákovice, Czech Republic	engraving	I
airbrush Fengda BD-207	Fengda, Zittau, Germany	spraying	I, III
ISO-TECH programmable power supply IPS-603	Northamptonshire, Great Britain	chip heating	I–IV
syringe pump Harvard apparatus 11 plus	Harvard Apparatus, Holliston, MA, USA	spray solvent/sample delivery	I, II, IV
syringe pump NE-300	New Era Pump Systems, USA	spray solvent delivery	III

digital infrared thermometer IR 1200-50D USB	Voltcraft, Hirschau, Germany	temperature measurement	I–III
rf krypton discharge photoionization lamp (PKR 106)	Heraeus Noblelight, Hanau, Germany	photoionization	I–IV
MANSON SDP- 2405	Manson, Kwai Chung, N.T., Hong Kong	power supply for lamp	I–III
glass plate cutter	CAMAG, Muttenz, Switzerland	adjusting TLC plate dimensions	II
Nanomat 4	CAMAG, Muttenz, Switzerland	sample application on TLC plates	II
Twin Trough chamber	CAMAG, Muttenz, Switzerland	preconditioning of TLC plates	II
PhotoMate APPI source	Syagen Technology, Tustin, CA, USA	APPI source	II
3D printer 3DWARF+	FUTUR3D, Prague, Czech Republic	printing of plastic objects	III

3.3 ION SOURCES

Two different home-built mass spectrometer ion sources were used in the work: (i) for the planar surface analysis (I, II, IV); (ii) for the nonplanar surface analysis (III). The former ion source consisted of a sample holder with a motorized stage movable in *xy*-directions (0–48 mm in *x*, 0–25 mm in *y*) (Figure 3.1A). The latter ion source consisted of a triangulation optoelectronic sensor ILD 1402-20 (MICRO-EPSILON, Ortenburg, Germany) for the sample height measurement, and a motorized sample stage movable in *xyz*-directions (0–75 mm in *x*, 0–25 mm in *y*, 0–20 mm in *z*) (Figure 3.1B). Both ion sources could be equipped with either DAPPI (I–IV) or DESI (III, IV). The position of the probe (microchip in DAPPI, or sprayer in DESI) was adjusted with a MX10R 4-axis miniature micromanipulator (Siskiyou Corporation, Grants Pass, OR, USA). The DAPPI

was introduced by Haapala[7] *et* al. in 2007 and the DESI by Takáts[6] *et* al. in 2004, and they both were used with only minor modifications to the original design.

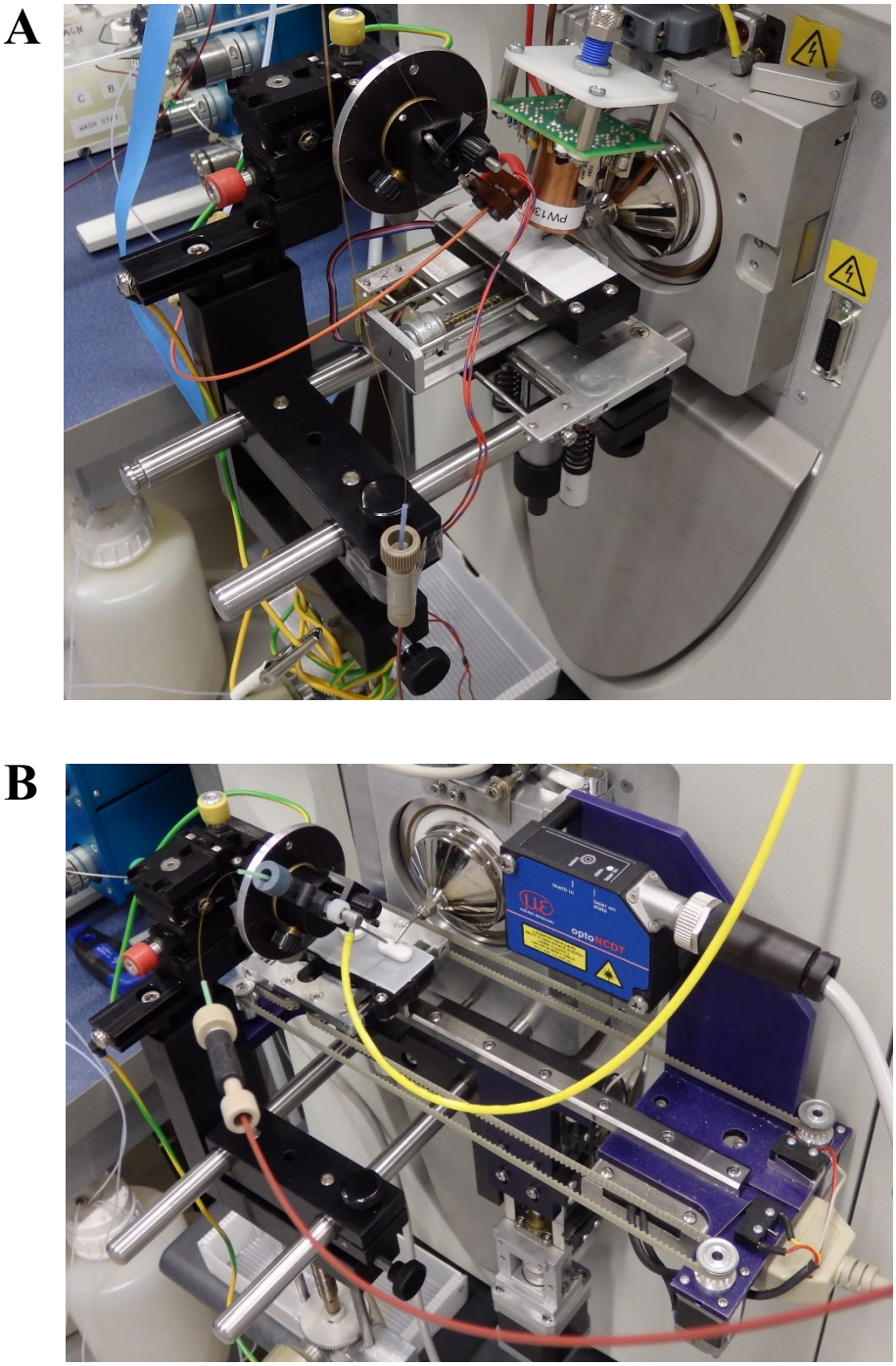

Figure 3.1. Photographs of the in-house built ion source for the (A) planar and (B) nonplanar surface analysis.

As for the ion source intended for the nonplanar samples, the entire experiment consisted of several steps as follows (Figure 3.2): (1) the sample height measurement

using a fixed laser sensor while the sample is moving in *x*- and *y*-directions; (2) calculation of coordinates for the stage movement from the sample height data; (3) moving the sample stage to the analytical position; (4) DESI-MS or DAPPI-MS data acquisition while the sample stage moves automatically in *xyz*-directions; and (5) data processing and visualization.

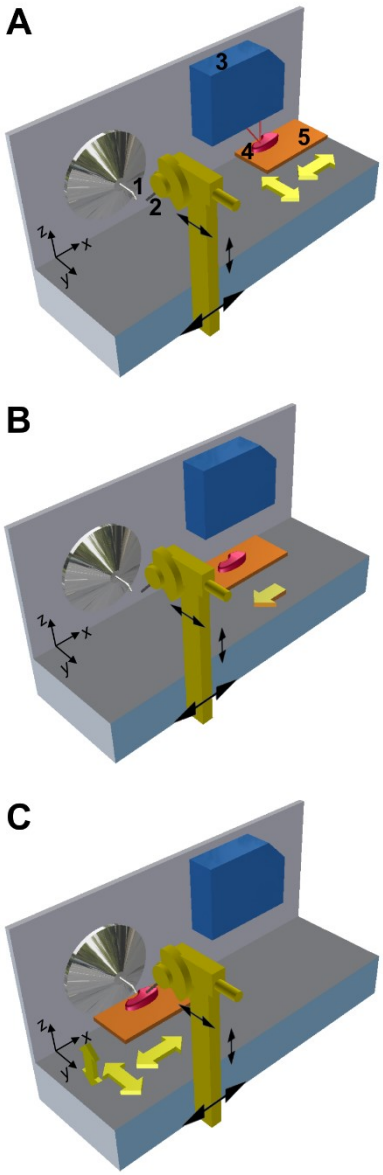

Figure 3.2. The scheme of the ion source showing the key steps of the measurement. (A) Height scanning position. 1: MS inlet capillary extension. 2: Probe (sprayer/microchip). 3: Laser sensor. 4: Sample. 5: Sample stage. (B) The sample moves to the analytical position. (C) Analytical position.

DAPPI source utilized custom-made heated nebulizer microchips provided by the Mass spectrometry and metabolomics group (T. J. Kauppila group), Faculty of Pharmacy,

University of Helsinki. The manufacturing of the microchips has been described in detail previously.[65] In this work, the nebulizer microchips were used to provide a heated, confined jet of solvent vapor. The temperature of the heated jet can be chosen by changing the microchip heating power; the maximum jet temperature is approx. 350 ºC. The solvent and nebulizer gas flow rates and estimates of the applied temperatures are given in the original publications.

In DESI, two different home-built sprayers were used for the measurements. The first type of sprayer (III, IV) consisted of two capillaries: the inner fused silica capillary for solvent (i.d. 100 µm, o.d. 365 µm), and the outer stainless steel capillary for nitrogen (i.d. 500 µm, o.d. 1/16"). The solvent capillary was set at 4.5 kV. The second type of sprayer (IV) also consisted of two capillaries: the inner metal capillary for solvent (i.d. 83 µm, o.d. 184 µm) was grounded and the MS inlet capillary voltage was set at 2.5 kV. The i.d. of the outer (nitrogen) capillary was 0.25 mm.

4 RESULTS AND DISCUSSION

This section summarizes and discusses the results of the research. Details are provided in the original publications (I–IV).

4.1 THE DETECTION AND MAPPING OF THE SPATIAL DISTRIBUTION OF INSECT DEFENSE COMPOUNDS BY DESORPTION ATMOSPHERIC PRESSURE PHOTOIONIZATION ORBITRAP MASS SPECTROMETRY

Two chemically defended insect species were used as examples for the development of a new rapid analytical method based on desorption atmospheric pressure photoionization-mass spectrometry (DAPPI-MS). The distribution of defensive chemicals on the insect cuticle was examined. Since these chemicals are predominantly nonpolar, DAPPI was a suitable analytical method. Repeatability of DAPPI-MS signals and effects related to nonplanarity and roughness of samples were studied using acrylic sheets uniformly covered with an analyte. Chemicals present on the body surface were scanned along the median line of the insect from the head to the abdomen and vice versa, employing either the MS or MS^2 mode.

4.1.1 Defensive secretion components

The capability of DAPPI-MS to ionize insect defense compounds was first tested using the standards of (*E*)-1-nitropentadec-1-ene and unsaturated aldehydes (for structures see Figure 4.1). The DAPPI-MS spectra of (*E*)-1-nitropentadec-1-ene showed $[M + H]^+$ (*m*/*z* 256.2) and $[M - H]^-$ (*m*/*z* 254.2) ions in the positive and negative ion modes, respectively. The sensitivity in the negative ion mode appeared to be higher, likely because of an easy elimination of acidic hydrogens attached to double-bond carbons. The unsaturated

aldehydes (*E*)-hex-2-enal, (*E*)-oct-2-enal, (*E*,*E*)-deca-2,4-dienal, (*E*)-dec-2-enal and (*E*)-undec-2-enal provided protonated molecules at *m*/*z* 99.1, 127.1, 153.1, 155.1 and 169.2, respectively, in the positive ion mode (Figure 4.1).

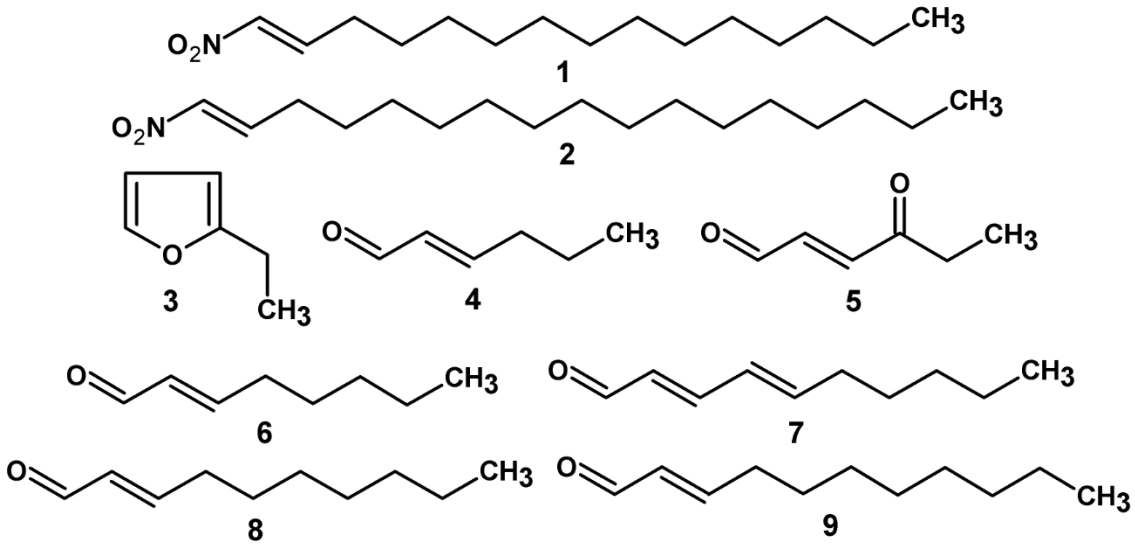

Figure 4.1. Structural formulas. 1: (*E*)-1-Nitropentadec-1-ene. 2: (*E*)-1-Nitroheptadec-1-ene. 3: 2-Ethylfuran. 4: (*E*)-Hex-2-enal. 5: (*E*)-4-Oxohex-2-enal. 6: (*E*)-Oct-2-enal. 7: (*E*,*E*)-Deca-2,4-dienal. 8: (*E*)-Dec-2-enal. 9: (*E*)-Undec-2-enal.

These defense chemicals were then searched in the insect samples. As the objective of this work was to analyze compounds directly on the insect cuticle, we investigated whether or not other cuticular compounds, mostly hydrocarbons, and lipids, have an impact on the detection of the target analytes. Therefore, we analyzed defensive chemicals in the whole-body extracts and also directly in the insect cuticle by focusing the hot solvent jet on the gland opening. Both the DAPPI-MS spectra of the body extracts and the spectra measured directly on the cuticle showed expected insect compounds, which indicated the power of DAPPI-MS to detect defensive compounds straight from the gland openings of the *P. simplex* soldier and *G. lineatum*. A list of identified compounds and high-resolution data are presented in Table 4.1.

Table 4.1. List of the compounds identified in the body extracts of the insects.

Compound	Measured *m/z*	Mass error [ppm]	Identification
(*E*)-1-nitropentadec-1-ene[a]	254.2121 ($[M - H]^-$)	2.6	exact mass and MS^2 against standard
(*E*)-1-nitroheptadec-1-ene[a]	282.2438 ($[M - H]^-$)	3.6	exact mass
2-ethylfuran[b]	97.0647 ($[M + H]^+$)	–0.9	exact mass
(*E*)-hex-2-enal[b]	99.0804 ($[M + H]^+$)	–0.6	exact mass and MS^2 against standard
(*E*)-4-oxohex-2-enal[b]	113.0597 ($[M + H]^+$)	–0.1	exact mass
(*E*)-oct-2-enal[b]	127.1118 ($[M + H]^+$)	0.4	exact mass and MS^2 against standard
(*E*,*E*)-deca-2,4-dienal[b]	153.1274 ($[M + H]^+$)	0.1	exact mass and MS^2 against standard
(*E*)-dec-2-enal[b]	155.1430 ($[M + H]^+$)	–0.2	exact mass and MS^2 against standard
(*E*)-undec-2-enal[b]	169.1587 ($[M + H]^+$)	–0.2	exact mass and MS^2 against standard

[a] *P. simplex*.

[b] *G. lineatum.*

The DAPPI-MS signals were found to rise linearly with increasing surface concentrations of (*E*)-dec-2-enal and (*E*)-1-nitropentadec-1-ene in the concentration ranges specified in Table 4.2. The limit of detection (LOD) values for (*E*)-dec-2-enal and (*E*)-1-nitropentadec-1-ene were 44 and 5 ng mm^{-2}, respectively (Table 4.2). Verapamil hydrochloride used as a benchmark compound showed predictably lower LOD than defense chemicals because it ionizes more readily (Table 4.2). The value determined here (0.10 ng mm^{-2}) was comparable to previous results (56 fmol, i.e. 0.03 ng) reported by Haapala et al.[7]

Table 4.2. The analytical figures of merit for standard compounds deposited on a PTFE film.

Compound	LOD [ng mm^{-2}]	Linear range[a] [ng mm^{-2}]	R^2
(*E*)-dec-2-enal	44	44 – 4920 (7)	0.9854
(*E*)-1-nitropentadec-1-ene	5	5 – 141 (4)	0.9782
verapamil hydrochloride	0.1	0.1 – 3.6 (7)	0.9600

[a] The number of data points is indicated in brackets.

4.1.2 Surface effects in DAPPI-MS

Ambient spray desorption techniques are known for limited scan-to-scan repeatability and substantial effects of geometrical arrangement on the results. Obtaining reproducible results be- comes even more challenging when the sample is not perfectly planar and smooth. Insects are objects that are generally nonplanar. They possess segmented bodies supported by an exoskeleton and their surface shows a great variety of morphologically distinct features of various diameters. These features may affect the signal intensities and generate a bias in profile data or mass images. Therefore, several experiments were carried out to evaluate the influence of the surface roughness.

Plain surface covered with verapamil hydrochloride and tilted ca. 6° from the horizontal position (Figure 4.2A) was used to evaluate the effect of a vertical distance between the sample surface and inlet capillary. We found a small decrease of signal intensity for the distances within 0–0.6 mm range, but significantly higher signal drop for larger distances (Figure 4.2B). Therefore, sample features with the dimensions (heights) up to 0.6 mm do not have a strong effect on the signal. The investigated insect specimens were scanned along the median line. When an ideal line was projected on the dorsal surface of *P. simplex* soldier, the maximum distance between the body surface and the ideal line was about 0.5 mm. It suggests that termite surface along the median line is not remarkably different from a plane and the data should not be biased. As for *G. lineatum*, maximum distance 1.8 mm was found at the abdominal tip, which indicated marked a decrease of the signal intensity. However, the scent glands and their reservoirs are located in the posterior part of the thorax and anterior abdomen, where the distance did not exceed 0.6 mm. The signal intensity in this area would not be greatly affected by the sample-to-inlet distance.

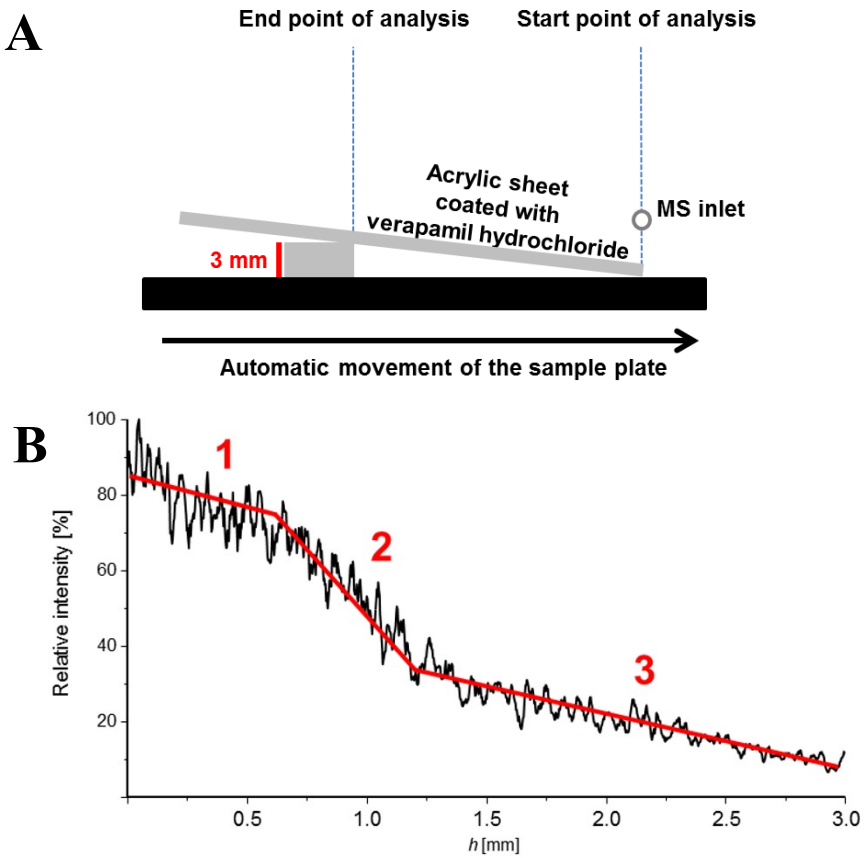

Figure 4.2. (A) The experiment setup for evaluating the effect of distance between the sample surface and inlet capillary. (B) A graph of the signal intensity against the distance between the MS inlet capillary extension and the acrylic sheet coated with verapamil hydrochloride. The curve was averaged from 8 measurements.

4.1.3 Spatial distribution of defensive compounds

In order to localize the exact position of the gland opening, we monitored the spatial distribution of the defense secretion on the insect cuticle, assuming that the highest signal comes from the gland opening. As the model species (as well as many other insects) have the glands located in the central part of the body, an MS profiling along the median line of the insect specimens was used. The termite frontal gland was monitored using the (*E*)-1-nitropentadec-1-ene ions $[M - H]^-$ (MS) and $[M - H - H_2O]^-$ (MS^2), whereas the stink bug gland opening was visualized using the unsaturated aldehyde ions $[M + H]^+$ (MS) and $[M + H - H_2O]^+$ (MS^2). The microchip heater power was set sufficiently high to ensure effective desorption of the analytes, but not so high as to cause damage to the insect cuticle. We finally used a microchip heater power of 1.2 W (effective jet

temperature ≈ 80 °C) for the termite and 4.5 W (effective jet temperature ≈ 200 °C) for the stink bug with a more heat-resistant cuticle. In order to verify that the defensive compounds had not been significantly redistributed by the hot jet, we performed the measurements twice, from the head to the abdomen (forward analysis), and vice versa (backward analysis). Each experiment was performed with a new insect specimen and smoothing was enabled in data post-processing.

The signal maxima of (*E*)-1-nitropentadec-1-ene appeared approximately 2 mm from the tip of the termite mandibles (Figure 4.3). As for the *G. lineatum*, the signal maxima of the selected unsaturated aldehydes were localized 4–5 mm from the head. These distances matched very closely the real positions of the gland openings on the insects. The signal maxima reliably indicated the positions of the gland openings, but the defense compounds were usually detected from a significantly wider area on the insect surface. The wider distribution likely reflected the natural presence of the defense compounds on the cuticle in the vicinity of the gland opening, but carry-over of volatile analytes cannot be entirely excluded. As the signals were also elevated in the areas of the gland reservoirs, we assumed it was caused by the disruption of the cuticle. I did not attempt to perform experiments with living specimens because the conditions used were not consistent with surviving of the investigated insects. The localization of the gland openings in insects can be complicated by their nonplanarity. Fortunately, the surface along the median line of insects is usually more or less flat, which makes the compound profiling relatively easy in many cases. As evident from the experiments described above, a small change of the sample-to-inlet distance does not affect signals significantly. However, for longer distances (more than ca. 0.6 mm), the measured signal drops significantly. For such objects, the sample needs to be moved also along the *z* axis to ensure an optimum geometry for each sampling spot on the cuticle.

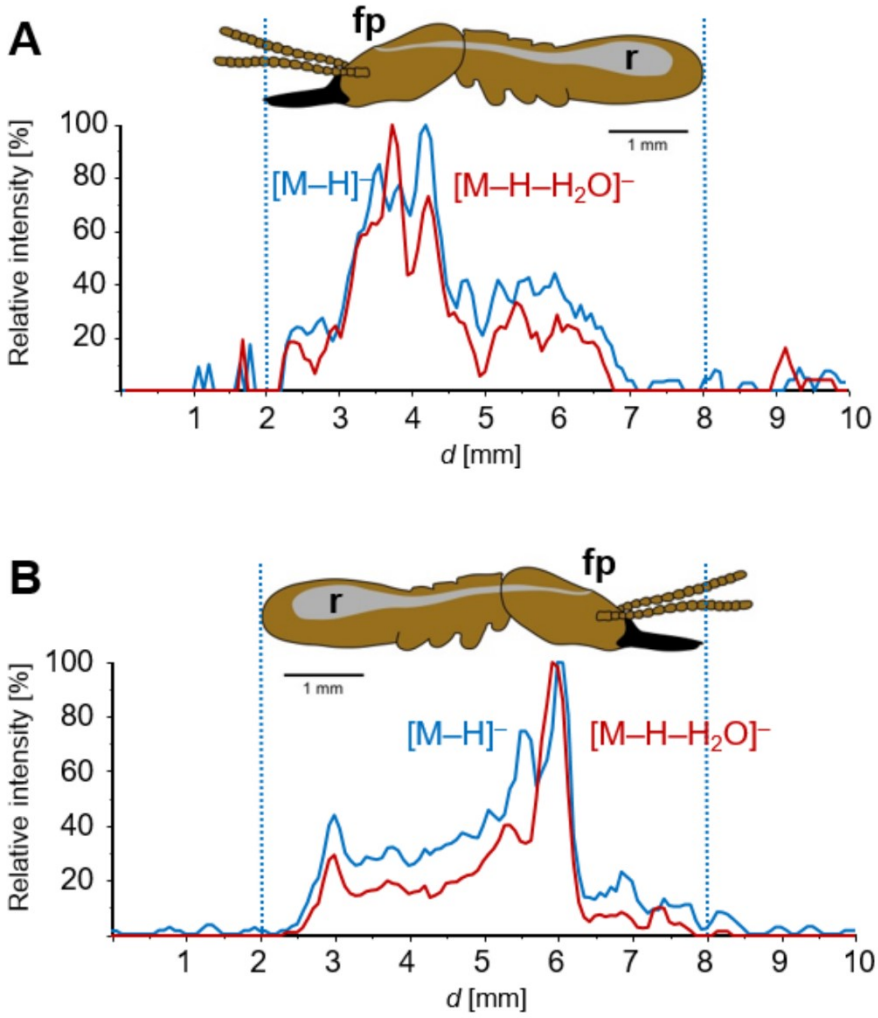

Figure 4.3. Ion traces of (*E*)-1-nitropentadec-1-ene recorded along the median line of a *P. simplex* soldier (the posterior side). fp: Frontal pore (fontanelle). r: Reservoir. (A) Forward analysis (from the head to the abdomen). (B) Backward analysis (from the abdomen to the head). The blue line: $[M - H]^-$ in the full-scan spectrum (*m*/*z*: 254.20–254.22). The red line: $[M + H - H_2O]^-$ in the MS^2 spectrum (*m*/*z*: 236.19–236.21). The MS and MS^2 spectra were acquired simultaneously.

4.2 THIN-LAYER CHROMATOGRAPHY/DESORPTION ATMOSPHERIC PRESSURE PHOTOIONIZATION ORBITRAP MASS SPECTROMETRY OF LIPIDS

Desorption atmospheric pressure photoionization (DAPPI) allows surface analysis in the open atmosphere and is thus an appropriate method for the direct coupling of thin-layer

chromatography (TLC) and mass spectrometry (MS). Therefore, the power of DAPPI-MS for ionizing and detecting lipids from TLC and high-performance thin-layer chromatography (HPTLC) plates in MS and MS^2 modes was tested. TLC/DAPPI-MS was applied for lipids of vernix caseosa, a white creamy proteolipid biofilm that progressively coats the fetus during the last trimester of the pregnancy, and plant oils including caraway, parsley, safflower, and jojoba oils. Various lipids were identified by means of high resolution/accurate mass measurement of Orbitrap and comparison of the retardation factors with standards. Lipid class separation was carried out on the NP-HPTLC plates, whereas individual triacylglycerol and wax ester species were separated on the reversed-phase HPTLC plates.

4.2.1 TLC/DAPPI-MS of lipid standards

The ability of DAPPI to desorb and ionize cholesterol, 1,3-dipalmitoyl-2-oleoyl-glycerol, 1,2-dioleoyl-hexadecane-1,2-diol, palmityl oleate, cholesteryl oleate, and squalene from unprocessed normal-phase (NP)-HPTLC plates was investigated first. When compared to common DAPPI-MS conditions, a relatively high microchip heating power (6.5 W; effective jet temperature ≈ 240 °C) was required for effective desorption of large lipid molecules. Chloroform in the spray solvent enhanced the desorption of lipids, and ammonium formate ensured the formation of ammonium adducts of species with low proton affinity. Besides protonated molecules and ammonium adducts, ions created by hydride abstraction and/or expectable fragments were observed (Table 4.3).

In the next step, the lipid standards were chromatographically separated. The mobile phase containing 95% of hexane, 5% of diethyl ether, and 1% of acetic acid turned out to be the most suitable for separating the model lipids on silica gel.[66] The chromatograms of a mixture of six lipid standards separated on the NP-HPTLC and NP-TLC plates are shown in Figure 4.4. The retention order was the same on both plates and agreed with earlier reported data.[66] However, different R_f values were obtained with the different plates: apart from squalene, the analytes migrated more slowly on the NP-TLC plate. In agreement with the literature,[66] palmityl oleate (violet line) and cholesteryl oleate (blue line) partly overlapped in both systems (chromatographic resolution R_S = 0.45 for the NP-HPTLC plate and R_S = 0.41 for the NP-TLC plate). Assessment of the DAPPI-

MS detection of the analytes separated on the NP-HPTLC and the NP-TLC plates was done based on LODs that were ranging from 15 to 1000 ng (Table 4.3). The LODs for two different TLC plate types were virtually identical, but the values differed significantly between the investigated lipids. The LOD values in this analytical setup reflected (i) ionization efficiency by APPI and (ii) desorption efficiency of the analytes from the surface. To get an insight into these factors, direct-infusion APPI-MS and TLC/DAPPI-MS data were compared.

Table 4.3. The ions observed in DAPPI spectra of the lipid standards desorbed from the NP-HPTLC plate, and LODs of the lipid standards separated on the NP-HPTLC and NP-TLC plates.

Compound	***m/z* (ion identity; relative intensity)**	**LOD [ng]; [pmol]**	
		NP-HPTLC	**NP-TLC**
cholesterol	383.3 ($[M - 3H]^+$; 100); 385.3 ($[M - H]^+$; 54); 367.3 ($[M - H - H_2O]^+$; 21)	15; 39	15; 39
1,3-dipalmitoyl-2-oleoyl-glycerol	577.5 ($[M + H - C16:0]^+$; 100); 551.5 ($[M + H - C18:1]^+$; 79); 850.8 ($[M + NH_4]^+$; 22)	1000; 1200	1000; 1200
1,2-dioleoyl-hexadecane-1,2-diol	804.8 ($[M + NH_4]^+$; 100); 505.5 ($[M + H - C18:1]^+$; 99)	400; 508	400; 508
palmityl oleate	507.5 ($[M + H]^+$; 100); 524.5 ($[M + NH_4]^+$; 50); 283.3 ($[M + H - C_{16}H_{32}]^+$; 48)	100; 197	100; 197
cholesteryl oleate	369.4 ($[M + H - C18:1]^+$; 100); 383.3 ($[M + H - C_{18}H_{36}O]^+$; 58)	30; 46	25; 38
squalene	409.4 ($[M - H]^+$; 100); 411.4 ($[M + H]^+$; 98)	45; 110	50; 122

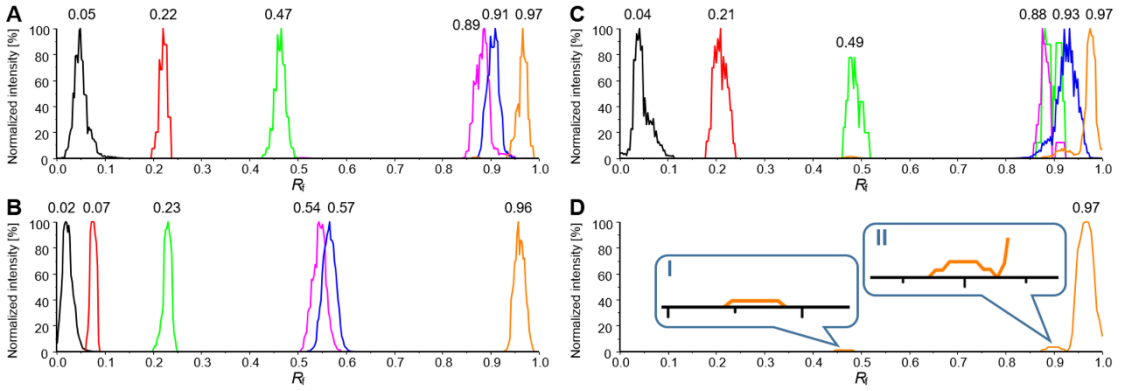

Figure 4.4. Extracted ion chromatograms acquired by DAPPI-MS. TLC mobile phase: hexane/diethyl ether/acetic acid (95:5:1; v/v/v). Model lipid mixture in MS mode from (A) the NP-HPTLC plate and (B) the NP-TLC plate. The black line: cholesterol $[M - 3H]^+$. The red line: 1,3-dipalmitoyl-2-oleoyl-glycerol $[M + H - C16:0]^+$. The green line: 1,2-dioleoyl-hexadecane-1,2-diol $[M + NH_4]^+$. The violet line: palmityl oleate $[M + H]^+$. The blue line: cholesteryl oleate $[M + H - C18:1]^+$. The orange line: squalene $[M - H]^+$. (C) Total lipid extract of vernix caseosa from the NP-HPTLC plate in MS mode. The green line: first peak (R_f = 0.49), palmitoyl-oleoyl-docosane-1,2-diol $[M + H - C16:0]^+$; second peak (R_f = 0.88), WE 40:2 $[M + H]^+$. (D) Total lipid extract of vernix caseosa from the NP-HPTLC plate in MS^2 mode. The orange line: squalene $[M - H - C_{13}H_{24}]^+$ product ion. (I) 2,3-Oxidosqualene. (II) Unidentified compound.

The experiments were carried out with two homologous series of wax esters. Equimolar solutions of saturated and monounsaturated wax esters with 26−44 and 26−40 carbon atoms, respectively, were infused into the APPI source. For both series, the signal of $[M + H]^+$ detected by APPI-MS increased with the total number of carbons, i.e., with the molecular weight of wax ester; however, the same compounds exhibited completely opposite behavior when desorbed from the TLC plate (Figure 4.5A,B). Clearly, the desorption efficiency of the analytes from the TLC plate rapidly decreased with the molecular weight (total number of carbons) of wax esters. This effect was observed for both saturated and unsaturated wax esters. An added experiment with wax esters having 36 carbons and up to 4 double bonds confirmed increasing ionization efficiencies with the number of double bonds. As both APPI-MS and DAPPI-MS data showed similar sensitivity dependence on the number of double bonds (Figure 4.5C), the effect of the number of double bonds on the desorption efficiency was considered small or negligible. Next, the APPI-MS response was measured for lipid standards representing various lipid classes. Briefly, the ionization efficiency (APPI-MS response) increased as follows: squalene < palmityl oleate < cholesterol < cholesteryl oleate < 1,2-dioleoyl-hexadecane-

1,2- diol < 1,3-dipalmitoyl-2-oleoyl-glycerol. This order did not follow the LODs with TLC/DAPPI-MS reported in Table 4.3; in fact, it was roughly opposite. Lipids with higher molecular weight were effectively detected by APPI-MS, but their high LODs in TLC/DAPPI-MS suggested ineffective desorption from the silica gel surface. Data from these experiments clearly demonstrated a crucial role of the desorption step in TLC/DAPPI-MS, particularly for heavier lipids. The desorption efficiency depends on both the spray jet temperature and the chemical composition of the spray solvent; therefore, these parameters need to be carefully optimized for optimum results.

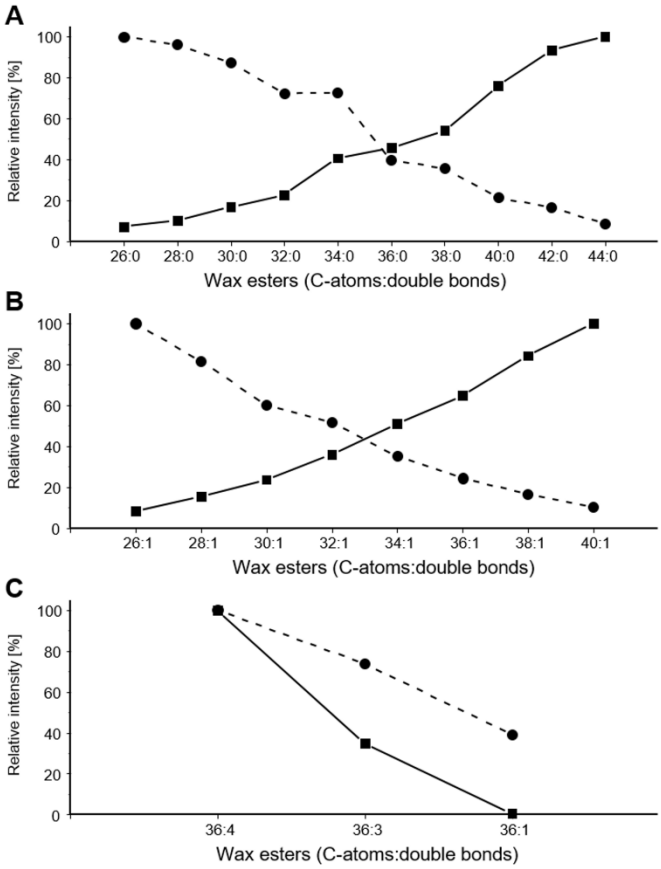

Figure 4.5. The relative intensity of signals of wax esters in the equimolar mixtures measured by APPI-MS (solid lines) or desorbed from the NP-HPTLC plate without chromatographic separation and measured by DAPPI-MS (dashed lines). (A) Saturated wax esters with different chain lengths: laurates (26:0−34:0) and behenates (36:0−44:0). (B) Monounsaturated wax esters with different chain lengths: myristoleate (26:1), palmitoleate (28:1), and oleates (30:1−40:1). (C) Wax esters with equal chain lengths and different numbers of double bonds: 16:0−20:4n-6 (36:4); 18:0−18:3n-3 (36:3); 18:0−18:1n-9 (36:1).

4.2.2 TLC/DAPPI-MS of vernix caseosa lipids

Next, the TLC/DAPPI-MS method was applied to the analysis of vernix caseosa lipids. The investigated standards were evaluated by using the total lipid extract separated on the NP- HPTLC plate. The structures of the lipids were confirmed using accurate masses in the full-scan spectra, the CID MS^2 spectra, and the R_f values.

The total lipid extract of vernix caseosa showed signals for all the investigated analytes, except for 1,2-dioleoyl-hexadecane-1,2-diol. This is not surprising, as this particular 1,2-diol diester has not been reported to be present in vernix caseosa.[61] One of the most abundant molecular species of 1,2-diol diesters in vernix caseosa is palmitoyl-oleoyl-docosane-1,2-diol,[61] which was also successfully detected by TLC/DAPPI-MS (Figure 4.4C, green line; R_f = 0.49). The squalene trace (orange line) showed two additional weak signals approximately in the middle (R_f = 0.48) and near the front (R_f = 0.91) of the plate (Figure 4.4C,D). The full scan spectrum of the first peak (R_f = 0.48) showed, besides *m/z* 409.4, also a more abundant *m/z* 427.4. The elemental composition of *m/z* 427.4 ($C_{30}H_{51}O$) indicated an oxidation product of squalene. We hypothesized that this substance could be 2,3-oxidosqualene, an important precursor in the biosynthesis of sterols.[67] Our previous, and so far unpublished, GC/MS experiments unambiguously demonstrated the presence of this compound in the total lipid extract of vernix caseosa. To test the hypothesis, we analyzed the model lipid mixture with the added standard of 2,3-oxidosqualene. Indeed, the spectra and the retardation factors of the unknown peak R_f = 0.48 and 2,3-oxidosqualene matched. The second peak (R_f = 0.91), however, was not identified. It is worth noting that 2,3-oxidosqualene could not be distinguished without separation from the squalene oxidation product formed in the ionization process, which illustrates benefits of the ambient ionizations combined with TLC.

4.2.3 TLC/DAPPI-MS of plant oils

Four oils, namely, caraway, parsley, safflower, and jojoba oil, were investigated. The characterization of compounds was based on the accurate mass measurements and the known composition of plant oils.[68,69]

Apart from jojoba oil, the plant oils showed intense signals for the $[M + NH_4]^+$ adducts of triacylglycerols (prevalently composed of C16:0, C18:0, C18:1, and C18:2 fatty acid chains) and fragments. The results were in good agreement with an earlier report[68] dealing with the composition of plant oils. The mass spectra of jojoba oil affirmed that it differs entirely from other plant oils by its chemical composition, being a mixture of wax esters,[69] which were detected as $[M + H]^+$ ions in DAPPI-MS.

NP-TLC is generally recognized as a useful tool for the isolation and purification of triacylglycerols from the natural lipid mixtures but with a very limited capability to separate individual triacylglycerol species.[70] Nevertheless, a fairly good separation on the NP-HPTLC plate was observed for abundant triacylglycerols (TG 54:6, TG 52:4, and TG 54:3) in caraway oil (Figure 4.6A) as well as in parsley and safflower oils. Owing to the adsorption separation mechanisms on the polar stationary phase, the retardation factors decreased with the polarity, i.e., mainly with the number of double bonds. The retention order was in agreement with an earlier work investigating NP-HPLC of triacylglycerols.[71] Abundant molecular species of wax esters in jojoba oil (Figure 4.6C), all with the same number of double bonds (WE 38:2, WE 40:2, WE 42:2, and WE 44:2), were less efficiently separated because the polarity differences given only by the variations in the chain lengths were smaller.

Next, reversed-phase (RP)-TLC, which is a common method applicable for the separation of individual molecular species of lipids,[70] was studied. The mobile phase containing 90% of acetone and 10% of acetonitrile turned out to be the most suitable for the separation of triacylglycerols and wax esters (Figure 4.6B,D). Predictably, the analytes migrated in the ascending order of the equivalent carbon number (ECN, defined as the actual number of carbon atoms in the aliphatic residues minus twice the number of double bonds per molecule) due to the partition separation mechanism. Clearly, the chromatographic resolution for the examined lipids was significantly enhanced. Broad peaks were observed for some triacylglycerols, from both NP- and RP-HPLTC plates (Figure 4.6A,B). These peaks were likely to be composed of several partially separated species with the same masses.

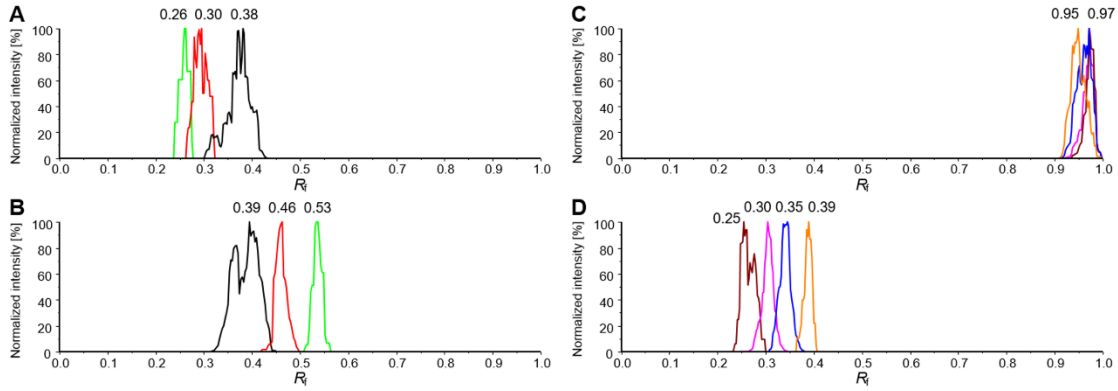

Figure 4.6. Extracted ion chromatograms acquired by DAPPI-MS in MS mode. Caraway oil from (A) the NP-HPTLC and (B) the RP-HPTLC plate. Jojoba oil from (C) the NP-HPTLC and (D) the RP-HPTLC plate. TLC mobile phases for the NP-HPTLC plate, hexane/diethyl ether/acetic acid (93:7:1; v/v/v), and the RP-HPTLC plate, acetone/acetonitrile (90:10; v/v). The green line: TG 54:6 $[M + NH_4]^+$. The red line: TG 52:4 $[M + NH_4]^+$. The black line: TG 54:3 $[M + NH_4]^+$. The orange line: WE 38:2 $[M + H]^+$. The blue line: WE 40:2 $[M + H]^+$. The violet line: WE 42:2 $[M + H]^+$. The brown line: WE 44:2 $[M + H]^+$.

4.3 ION SOURCE WITH LASER TRIANGULATION FOR AMBIENT MASS SPECTROMETRY OF NONPLANAR SAMPLES

The analysis of nonplanar samples in ambient mass spectrometry poses a formidable challenge. Here, an ion source equipped with laser triangulation for analyzing nonplanar surfaces was constructed. It was designed as a two-position device, where the sample height was measured using laser triangulation and the target compounds were then analyzed. Thanks to a stage movable in *xyz* the ion source maintained an optimal vertical distance between the sample and sampling capillary for each measured spot during the surface analysis. The *xyz*-coordinates for the movement of the sample stage were computed using the laser sensor data in such a way to avoid direct contact of the sampling capillary and the measured surface. Chemicals on the surface of nonplanar samples were probed along a line extending across the surface of the measured objects.

4.3.1 Design and software control of the ion source

The ion source was designed as a two-position device, with the height-measuring site shifted 12.5 cm horizontally from the ionization region. Such an arrangement made it possible to keep the space in front of the entrance capillary empty and operate the device in DESI or DAPPI at optimum geometry without space restrictions. The entire experiment consisted of several steps as follows: (1) the sample height measurement using a fixed laser sensor while the sample is moving in the *x*- and *y*-directions, (2) calculation of the coordinates for the stage movement from the sample height data, (3) moving the sample stage to the analytical position, (4) DESI-MS or DAPPI-MS data acquisition while the sample stage moves automatically in *xyz*-directions, and (5) data processing and visualization.

The sample height across its surface was measured using a contactless optical triangulation sensor. The sensor used in this work made it possible to measure object heights up to 20 mm. In this range, the measured height resolution was better than 10 µm, and the angle between the emitted and the detected light beam was 26–31°. The correct measurement with a triangulation sensor requires that the reflected light freely reach the receiver (Figure 4.7A). However, morphological features with a high aspect ratio (e.g. protrusions or depressions) near the measured position may shield the reflected light, which prevents the height value being recorded (Figure 4.7B). In such cases, an interpolation algorithm was applied to calculate the missing points from the neighboring spots.

The sample height values measured by the laser sensor were converted into *xyz*-coordinates for the sample stage movement. The coordinates were adjusted to prevent eventual hitting the sample, especially near morphological features with a high aspect ratio. The problem is illustrated in Figures 4.7C and 4.7D, which show a hypothetical cut across the sample in the *xz* plain and thus simulates sample profiling along a line. The purple line denotes the *z*-coordinates provided by the laser sensor for the optimum surface-to-capillary distance in the *z*-axis. The initial position of the sample stage in the *z*-axis was adjusted manually. If the sample stage was moved so that the capillary followed the purple line in the Figure 4.7C, then the protrusion of the sample would hit the sampling capillary. Therefore, an adjustment considering the capillary diameter

(defined by the user in the control software) had to be applied (the blue line). In other words, the value in the *z*-axis was modified in the horizontal proximity of the morphological features. After this adjustment, the sampling capillary stays slightly distant from the surface in the critical areas near the high-aspect ratio features thus protecting the sample from being touch by the capillary. Similar adjustments were also applied to the sample areas featuring depressions narrower than the diameter of the sampling capillary (Figure 4.7D). The algorithm calculating the corrected coordinates has been reliably developed only for a measurement along a line across a sample.

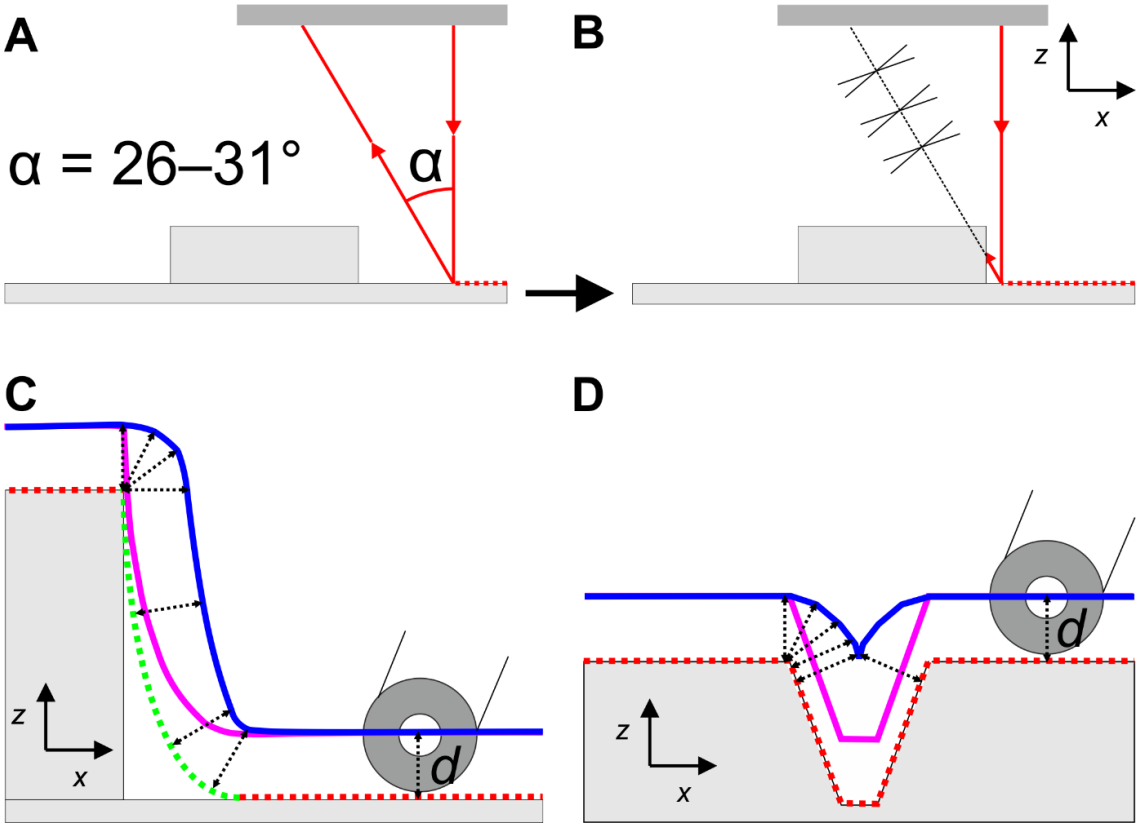

Figure 4.7. Scheme of the height measuring (A and B) and calculation of the coordinates for sample stage movement (C and D). (A) The angle between the emitted and the detected light beam was 26–31°. (B) Some morphological features near the measured position may shield the reflected light, which prevents the height value being recorded. (C) Calculation of coordinates near a protrusion. (D) Calculation of coordinates near a depression narrower than the diameter of the sampling capillary. The red line denotes laser beam. The red dotted line denotes points that were correctly measured by the sensor. The green dotted line denotes points that were interpolated. The purple line denotes the uncorrected *z*-coordinates of the sampling capillary that inevitably results in hitting the sample. The blue line denotes the final *z*-coordinates for the sample stage movement.

4.3.2 Testing the ion source with geometric shapes

The general performance of the ion source was tested in DESI mode using plastic objects covered by a thin layer of 2,5-dimethoxybenzoic acid. Three-dimensional solid objects of various shapes were profiled along their central line (Figure 4.8). The DESI sprayer remained in the same (optimum) position, while the sample stage moved in front of the sampling capillary. Two sets of experiments were performed. In the first set, the vertical position of the sample stage (*z*-coordinate) was fixed in such a way, that the highest point of the sample was at the optimum distance from the sampling capillary. In the course of measurement, the sample stage moved in the *x*-direction (*y*- and *z*-coordinates were fixed). In the case of the planar object, the surface remained in the same vertical distance from the sampling capillary and the analyte signal ($[M - H]^-$ at *m/z* 181.0) followed a horizontal line (Figure 4.9A). The relatively high signal variability (RSD 17.2%) was attributed to the inherently low stability of DESI, the inhomogeneity of the deposited layer, and the in-house construction of the sprayer. As regards the other objects, the signal was recorded only from their top regions that have reached the optimum distance with respect to the sampling capillary (Figures 4.9B-E).

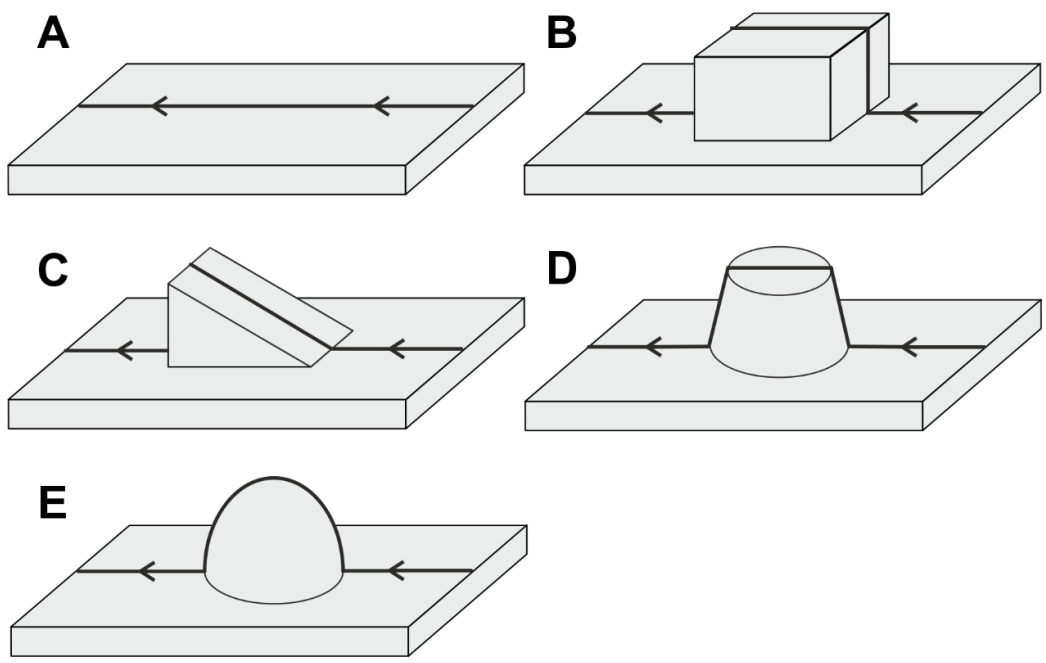

Figure 4.8. Printed plastic objects with marked analyzed line. (A) Plane. (B) Cuboid. (C) Inclined plane. (D) Truncated cone. (E) Spherical cap.

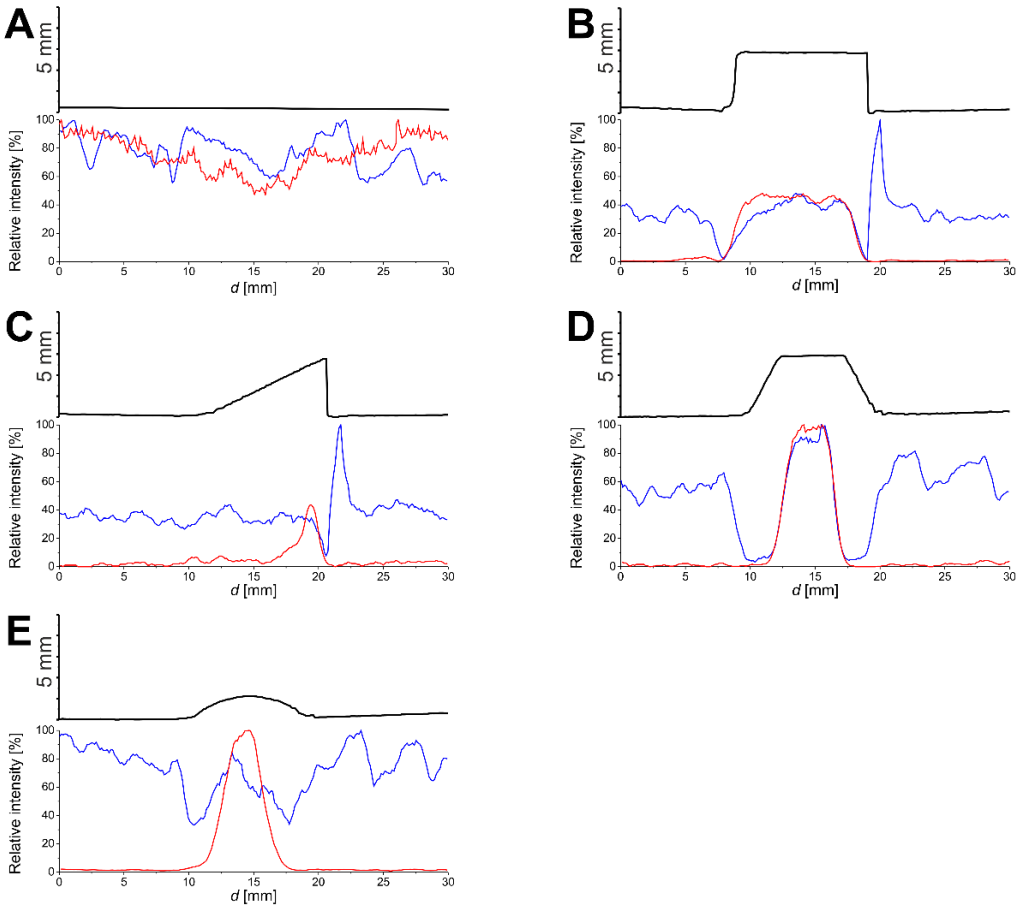

Figure 4.9. Extracted ion chromatograms acquired from the plastic objects coated with 2,5-dimethoxybenzoic acid ($[M - H]^-$ at *m*/*z* 181.0) by DESI-MS in the negative ion mode. The black line: the object profile measured by the laser sensor; the blue line: with automatic movement in *z*-axis; the red line: without automatic movement in the *z*-axis. (A) Plane. (B) Cuboid. (C) Inclined plane. (D) Truncated cone. (E) Spherical cap.

In the second set of experiments, the sample stage moved automatically in the vertical direction to keep the optimum distance from the sampling capillary for each measured point. In the course of measurement, the sample stage moved in the *x*- and *z*-directions (the *y*-coordinate was fixed). Because the sprayer-to-surface and surface-to-sampling capillary distances were the same throughout the measurement, a signal resembling a horizontal line was expected for all shapes. It was indeed the case for the plane (Figure 4.9), which was in fact in the same position as in the previous experiment. The signal variability was very similar to that recorded in the previous experiment (RSD 16.0%). For other shapes, the signal essentially followed a horizontal line as well, but

major disturbances were observed on the edges and slopes. The effect was less pronounced for the shapes with slowly changing height (inclined plane, spherical cap) and more significant for the objects with rapidly or abruptly changing its height (truncated cone, cuboid).

There are several effects that can be discussed relating to the observed disturbances on the object edges. The signal decrease can be explained by less efficient transport of desorbed ions from inclined surfaces into the mass spectrometer. The inclined surface elements may cause undesired reflections of desorbed droplets and direct them outside the sampling capillary. In the close vicinity of the objects, the desorbed droplets are also partially shielded by the object itself, which further decreases the ion transport. Furthermore, the homogeneity of the layer covering the plastic objects should be considered. Although the samples were prepared with great care, the sprayed layer can be less uniform on edges and inclined surfaces.

4.3.3 Applications

We proceeded with various food and pharmaceutical samples representing prospective applications of the ion source. The analyzed samples were nonplanar objects with irregular morphologies and heights between 4 and 7 mm. They were analyzed along a line extending across their surface, similar to the plastic objects described above. Depending on the chemical structure of analytes, either DESI or DAPPI was employed. In the first set of experiments, samples with a curved surface like coffee beans or Smarties were probed. The aim of the experiments was to demonstrate that the analytes can be detected from most of the surface. As shown in Figure 4.10, caffeine ($[M + H]^+$ at *m/z* 195.1) and citric acid ($[M - H]^-$ at *m/z* 191.0) provided significantly wider peaks when the automatic adjustment of the sample stage height was applied, and the peak width corresponded to the physical dimensions of the samples. These experiments confirmed that the automatic adjustment of the sample stage height made nonplanar samples more accessible for desorption and ionization. A higher number of spectra collected across a wider area offered more reliable information on the compounds present in the sample.

The second group of experiments concerned the simultaneous analysis of samples having different dimensions. Such an experimental setup is applicable for a high-

throughput measuring of samples that differ in size and shape, for instance, a simultaneous analysis of active ingredients in dissimilar pharmaceutical dosage forms (pills). To explore such applications, original samples and their smaller parts obtained by cutting were investigated by DAPPI-MS. Paramegal tablets and chewing gums were analyzed for the content of paracetamol ($[M + H]^+$ at m/z 152.1) and linoleic acid ($[M - H]^-$ at m/z 279.2), respectively (Figures 4.10C, D). As evident from the recorded traces, the signal from the smaller objects was low or even missing when the movement in the z-direction was not applied. By contrast, with the automatic adjustment of the sample stage height, both larger and smaller samples provided a roughly equal response.

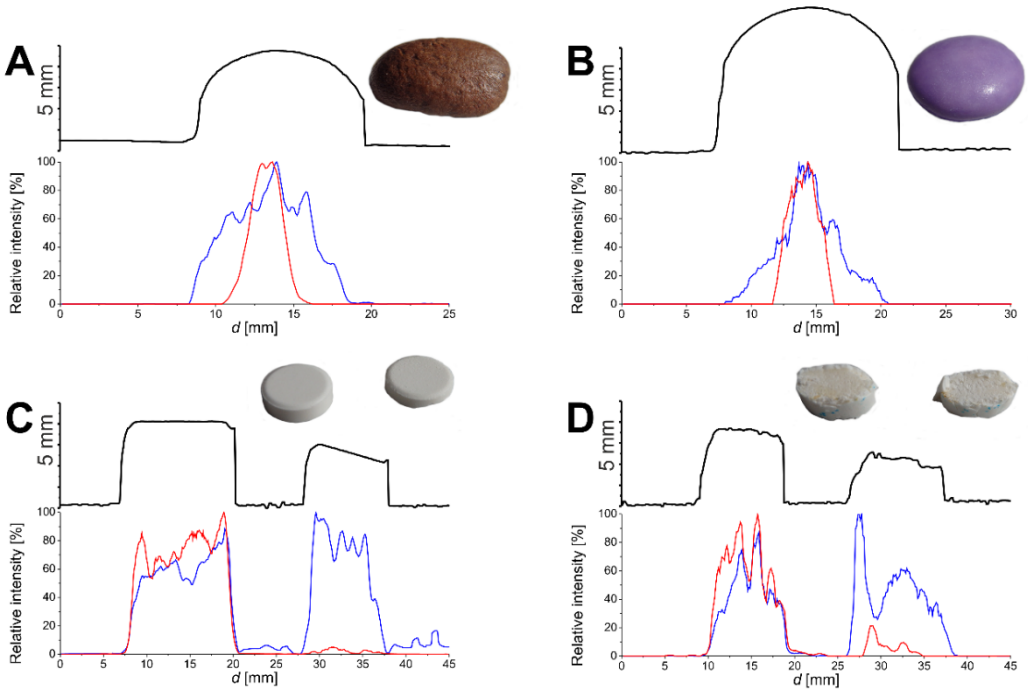

Figure 4.10. Extracted ion chromatograms (with illustrative pictures) acquired by DESI-MS (A, B) and DAPPI-MS (C, D) in the positive and negative ion modes. The black line: the sample profile measured by the laser sensor; the blue line: with automatic movement in the z-axis; the red line: without automatic movement in the z-axis. (A) Caffeine $[M + H]^+$ (m/z 195.1) from a coffee bean. (B) Citric acid $[M - H]^-$ (m/z 191.0) from a Smartie. (C) Paracetamol $[M + H]^+$ (m/z 152.1) from Paramegal tablets. (D) Linoleic acid $[M - H]^-$ (m/z 279.2) from chewing gums.

4.4 FEASIBILITY OF DESORPTION ATMOSPHERIC PRESSURE PHOTOIONIZATION AND DESORPTION ELECTROSPRAY IONIZATION MASS SPECTROMETRY TO MONITOR URINARY STEROID METABOLITES DURING PREGNANCY

Steroids have important roles in the progress of pregnancy, and their study in maternal urine is a non-invasive method to monitor the steroid metabolome and its possible abnormalities. We explored the feasibility of two ambient mass spectrometry methods in steroid fingerprinting. Urine samples from pregnant women were screened by DESI and DAPPI Orbitrap high-resolution mass spectrometry (HRMS). The urine samples were processed by solid phase extraction for the DESI measurements and by enzymatic hydrolysis and liquid–liquid-extraction for DAPPI. Consequently, steroid glucuronides and sulfates were detected by negative ion mode DESI–HRMS, and free steroids by positive ion mode DAPPI–HRMS.

4.4.1 Qualitative results: ions observed by DAPPI–HRMS

The DAPPI urine spectra demonstrated abundant signals due to the background and endogenous compounds in the urine matrix. Since our study was aimed at screening pregnancy steroids, ions with *m/z* corresponding to calculated masses of steroid ions were given a closer look. Only a few signals were observed with noticeably higher absolute intensity from the non-pregnant samples compared to the water blanks: possible C19 steroids (androgens) at *m/z* 287.2005 ($[C_{19}H_{26}O_2 + H]^+$), and 289.2162 ($[C_{19}H_{28}O_2 + H]^+$), and a suspected C21 steroid peak at *m/z* 301.2525 ($[C_{21}H_{32}O + H]^+$). The late pregnancy samples showed abundant peaks for a huge group of suspected steroid ions (Table 4.4). The thermal energy needed to desorb the analytes in DAPPI and the APPI ionization process can produce several types of ions for steroids, such as $[M + H]^+$, $[M - H_2O + H]^+$, and $[M - 2H_2O + H]^+$ as earlier shown for pregnane derivatives,[72] estrogens,[73] corticosteroids,[74] and several other types of steroids[64,72,73] in APPI. Combined with the

inability to discern between isomers, the origins of the observed ions are problematic to identify in a complex mixture like urine. However, it can be confidently concluded that DAPPI detected C19 and C21 steroids corresponding to androgens, progestogens, and corticoids. The latter two are known to be important for pregnancy since they are metabolites of progesterone and cortisol, whereas C18 steroids, i.e., estrogens and their metabolites, which are also essential for pregnancy, are lacking in the spectra. This is most likely because free estrogens contain an acidic phenol group and have therefore low ionization efficiencies in positive ion mode. In addition, some of the studied samples (subject 1 day of gestation 235, 254, and subject 3 day of gestation 237) showed abundant signals for possible ions of pharmaceuticals such as the dimer of the painkiller paracetamol.

Table 4.4. Selected ions observed from the late pregnancy urine samples by LLE-DAPPI-HRMS and suspected to be due to steroid species. Observed *m/z* is the average of third trimester samples of subject 1 (day of gestation 194, 235, and 254). Corresponding compounds gives some but not all possible steroid ions at the observed *m/z*. For example, $[M - H]^+$ ions may form in DAPPI-MS but are excluded from the Table.

Observed *m/z*	**Tentative formula**	**Calculated *m/z***	**Δ*m/z* (mmu)**	**Corresponding compounds and notes**
283.24190	$[C_{21}H_{30} + H]^+$	283.24201	-0.11	pregn-4-en-3-one ($[M - H_2O + H]^+$)
287.20054	$[C_{19}H_{26}O_2 + H]^+$	287.20054	0.00	androstenedione ($[M + H]^+$)
292.23480	$[C_{19}H_{25}O_2D_3 + H]^+$	292.23502	-0.22	D_3-T (IS) ($[M + H]^+$)
299.23693	$[C_{21}H_{30}O + H]^+$	299.23692	0.01	tetrahydrodeoxycorticosterone ($[M - 2\ H_2O + H]^+$)
303.19543	$[C_{19}H_{26}O_3 + H]^+$	303.19545	-0.02	hydroxyandrostenedione/methoxyestradiol /oxotestosterone ($[M + H]^+$)
				cortisol ($[M - C_2H_3O_2]^+$)
305.21101	$[C_{19}H_{28}O_3 + H]^+$	305.2111	-0.09	ketoetiocholanolone/hydroxytestosterone/oxoandrostenediol/dihydroxyandrostenone/ hydroxydehydroepiandrosterone ($[M + H]^+$)
313.21624	$[C_{21}H_{28}O_2 + H]^+$	313.21619	0.05	hydroxyprogesterone/deoxycorticosterone ($[M - H_2O + H]^+$)
				progesterone/dehydropregnenolone ($[M - H]^+$)
315.23179	$[C_{21}H_{30}O_2 + H]^+$	315.23184	-0.05	progesterone/dehydropregnenolone

				($[M + H]^+$)
				tetrahydrocorticosterone ($[M – 2\ H_2O + H]^+$)
317.24747	$[C_{21}H_{32}O_2 + H]^+$	317.24749	-0.02	tetrahydrodeoxycorticosterone ($[M - H_2O + H]^+$)
319.26298	$[C_{21}H_{34}O_2 + H]^+$	319.26314	-0.16	pregnanetriol ($[M - H_2O + H]^+$)
331.22670	$[C_{21}H_{30}O_3 + H]^+$	331.22675	-0.05	hydroxyprogesterone/deoxycorticosterone ($[M + H]^+$)
				tetrahydrodehydrocorticosterone ($[M - H_2O + H]^+$)
337.27338	$[C_{21}H_{36}O_3 + H]^+$	337.27370	-0.32	pregnanetriol (MH^+)

4.4.2 Qualitative results: ions observed by DESI–HRMS

The main species in the negative ion DESI–HRMS spectra of the urine of non-pregnant subjects were suspected C19 steroid (androgen) sulfate and glucuronide, and C21 steroid (corticoid) glucuronide conjugate ions together with a few unidentified urinary chemicals. As in DAPPI, one should note that isomers and isobars cannot be separated by DESI–HRMS and therefore each detected *m*/*z* may represent several isobaric species. To evaluate the tentative assignments of DESI–HRMS spectra, DESI–QqQ-MS precursor ion scan was conducted following the precursors of *m*/*z* 97 to detect sulfates, and *m*/*z* 75, 85, and 113 to detect the glucuronides. The measurements confirm that the most abundant ions in the spectra are due to glucuronides and sulfates supporting the tentative assignments made for the HRMS data. The sensitivity of the QqQ-measurements was not as good as that of the HRMS measurements, and therefore some of the sulfates and glucuronides were not detected in the precursor ion mode.

The spectra of late pregnancy samples were plainly different from those of non-pregnant samples in the DESI experiments. Again, a DESI–QqQ-MS precursor ion scan was conducted with a sub-set of the samples, and the results support the tentative assignments of the most abundant sulfates and glucuronides observed.

Altogether, the spectra obtained with SPE–DESI–HRMS contain the conjugated forms of some of the abundant species in LLE–DAPPI–HRMS spectra: $C_{19}H_{28}O_3$, $C_{21}H_{34}O_2$, $C_{21}H_{32}O_3$, $C_{21}H_{34}O_3$, and $C_{21}H_{36}O_3$ were seen as conjugates in DESI and $[M + H]^+$ in DAPPI. Nevertheless, for the most part, the two techniques showed signals

for different species. This could be partly due to the fact that some steroids fragment in DAPPI. DESI also appeared more sensitive than DAPPI due to the lower background in DESI and possibly low ionization efficiency for, e.g., C18 steroids in DAPPI.

4.4.3 Steroid metabolite fingerprints at different stages of pregnancy

Once it was established that the DAPPI and DESI methods were able to detect changes occurring in urinary metabolites during the 2nd pregnancy of subject 1, person-to-person repeatabilities of the fingerprints of suspected pregnancy related steroid metabolites were evaluated. The normalized relative intensities for different ions are compared between samples given by different study subjects at the same phase of pregnancy in Figure 4.11. While the compared pairs gave roughly similar fingerprints except for the day 235 and 237 samples in DAPPI, according to a two tailed two sample *t*-test the normalized relative intensities were significantly different for most compared ions and sample pairs in both DAPPI and DESI (p = 0.05, for third trimester samples RSDs of normalized relative intensity, were below 61 and 63 % and average RSD was 20 and 18 % in DAPPI and DESI, respectively). This is expected, since even though pregnancy has a great impact on steroid excretion allowing easy distinguishing of non-pregnant samples from the pregnancy samples, natural biological variation related to age, stress, body mass index, and nutritional state/fasting cause variation in the study subjects' steroid metabolomes.[75] As will be discussed in the next section, the differences between studied individuals at the same phase of pregnancy are, however, small compared to changes occurring during the course of pregnancy.

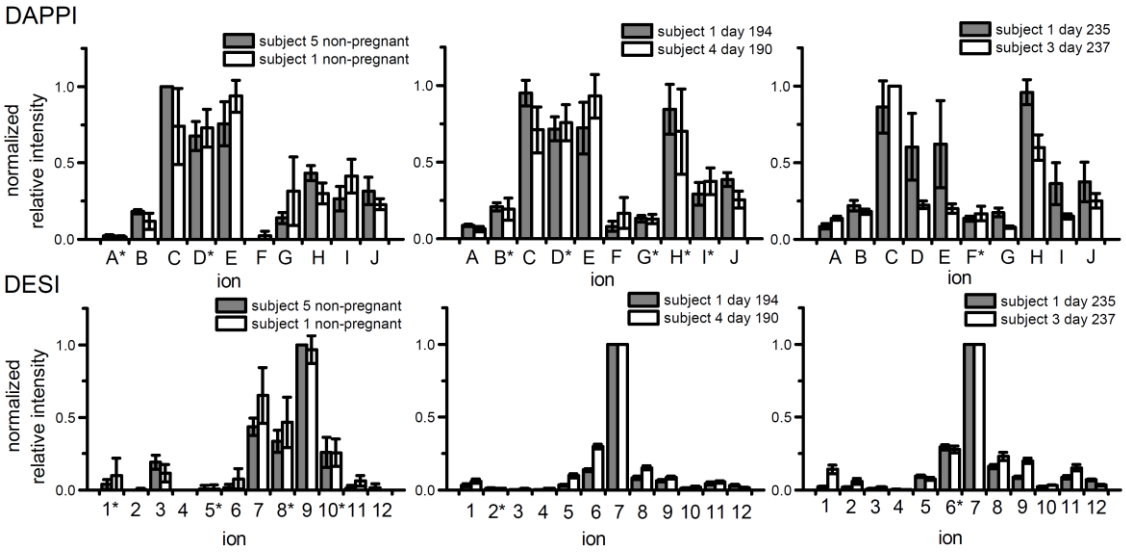

Figure 4.11. Examples of DAPPI and DESI steroid ion fingerprints presented as the average of normalized relative intensities. The ions are A: *m/z* 283.2419, B: 299.2369, C: 301.2526, D: 303.1954, E: 305.2110, F: 313.2162, G: 315.2318, H: 317.2475, I: 331.2267, J: 335.2580 in DAPPI and 1: 239.0851, 2: 300.6466, 3: 429.1951, 4: 461.1815, 5: 463.1972, 6: 493.2807, 7: 495.2963, 8: 509.2755, 9: 511.2911, 10: 525.2704, 11: 602.3001, and 12: 698.3754 in DESI. The error bars show standard deviations based on eight analyses.
* shows ions that did not have significantly different mean normalized relative intensity at $p = 0.05$ level for two studied subjects.

4.4.4 Steroid metabolites showing increase during pregnancy

The relative intensities of at least ten ions increased over an order of magnitude in the LLE–DAPPI–HRMS spectra as the 2nd pregnancy of subject 1 proceeded (Figure 4.12). These strongly pregnancy-related ions are most likely due to C21 steroid metabolites (progestins and corticoids) or C19 steroids (androgens). In DESI, at least twelve ions showed an order of magnitude increase of relative intensity (Figure 4.12), and most of them were suspected to be due to glucuronides and sulfates of C18 and C21 steroids (estrogens, progestins, and corticoids). The overall trends observed by both DAPPI and DESI are in agreement with the literature, as the production,[76] circulating,[77–79] and excreted[80] levels of estrogens, progestins, corticoids, and also many androgens are known to increase during pregnancy.

A detailed comparison of the DESI data was made with the previous study,[80] which reported longitudinal LC–MS data on urine samples from the 2nd pregnancy of subject 1 (day of gestation not matched with this study). Apart from estradiol

glucuronides, DESI was able to show increase for ions corresponding to all glucuronide species reported to show large, order(s) of magnitude increase in the LC–MS study.[80] However, the concentrations of three estriol glucuronides increase already in early pregnancy (day 10 of gestation compared to non-pregnant control) according to the earlier LC–MS study, but possibly due to insufficient sensitivity, the signal of the respective ion (*m*/*z* 463.1972) in the DESI spectra was not observed until day of gestation 108. Nevertheless, agreeing with the LC–MS results, the signal increased further from day 108 also according to DESI. Contrary to this, most species showing an increase during pregnancy in the DESI spectra were elevated already in the earliest pregnancy sample (day of gestation 24) compared to the control. This is in accordance with the previous study.[80]

The comparison of the DAPPI results with the previous LC–MS data[80] was not as straightforward as for DESI since the DAPPI signals represent free and hydrolyzed glucuronide and sulfate conjugates of the steroids, and the sulfates were not monitored in the LC–MS study. An increase of free or glucuronidated C21 steroids with six different molecular formulas, i.e. $C_{21}H_{30}O_2$, $C_{21}H_{34}O_2$, $C_{21}H_{34}O_3$, $C_{21}H_{36}O_3$, $C_{21}H_{36}O_2$, and $C_{21}H_{30}O_5$, was reported.[80] DAPPI–HRMS showed the increase of corresponding $[M + H]^+$ ion for two of the species, namely $C_{21}H_{30}O_2$ at *m*/*z* 315.2318, and $C_{21}H_{34}O_3$ at *m*/*z* 335.2580. It can be concluded, that DAPPI was unable to detect the increase of C18 steroids (estrogens). Whereas most detected pregnancy-related steroids demonstrated a large increase already in early pregnancy in DESI, DAPPI showed more of a steady growth with a clear maximum at the day of gestation 254. This may be due to the higher chemical background in DAPPI contributing to the early pregnancy signals, but it is also possible that the slope of signal response curve in DAPPI is low.

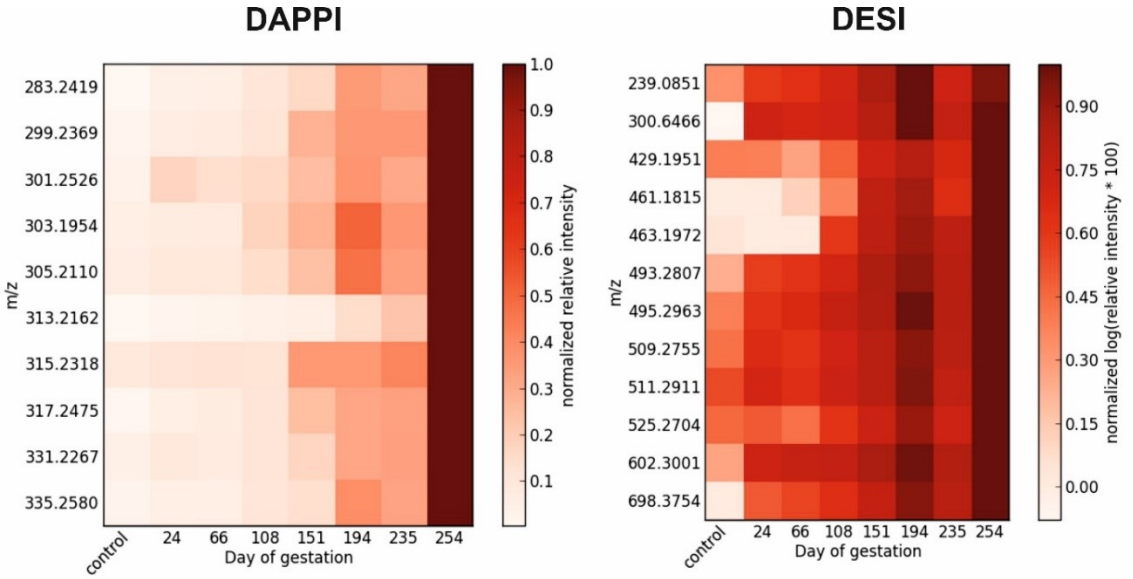

Figure 4.12. Heat map presenting changes of LLE-DAPPI-HRMS and SPE-DESI-HRMS response of selected ions during the second pregnancy of subject 1. In SPE–DESI–HRMS relative intensity was multiplied by 100, and logarithm was taken. The values for each ion were normalized by dividing by maximum value obtained for different studied days of gestation. Normalized value 1.00 corresponds to log(average($I(x)/I$(IS)) × 100) values between 2.6 and 5.0 and thus the figure shows over an order of magnitude change for all included ions. For the LLE–DAPPI–HRMS, the average relative intensity of each ion was divided by a maximum value obtained for different studied days of gestation.

5 CONCLUSIONS

The purpose of the research summarized in this doctoral thesis was development and applications of ambient mass spectrometry techniques. Thanks to the research, and the instrumental progress, this work enriches the field of ambient mass spectrometry and advances the frontiers of science. Firstly, the ambient ionization has been limited to the planar surface analysis. This project broadens the scope of ambient techniques towards the nonplanar surface analysis. Secondly, although many samples have been already analyzed by various ambient techniques, herein published practicable applications show a large amount of novelty. The future development of the ambient mass spectrometry in our laboratory could be focused on mass spectrometry imaging and improving the signal stability.

It was shown in the publication I that DAPPI combined with Orbitrap mass spectrometry can be successfully used to detect non-polar compounds produced by insects. It is a novel approach of localizing defensive gland openings, which was demonstrated for two insect models, the termite *Prorhinotermes simplex* and the stink bug *Graphosoma lineatum*. The compounds were profiled from the head to the abdomen and vice versa, employing both MS and MS^2 scans, to monitor their spatial distribution. The most intense signals correctly indicated the position of the gland openings and reservoirs in the insect models.

A new detection method based on DAPPI-MS for compounds separated by TLC has been introduced in the publication II. The feasibility of this approach has been demonstrated for neutral lipids commonly found in natural fats and oils. With regard to lipid class separation on silica gel (NP-TLC and NP-HPTLC), in terms of real plate number, the HPTLC plates exhibited more efficient separation. The reversed-phase separation system showed a fairly good separation of individual triacylglycerol and wax ester species. This study showed a strong effect of the analyte molecular weight on the desorption efficiency from the TLC plates, which requires careful optimization of the experimental parameters, especially the desorption temperature. Ambient ionization techniques, such as DAPPI-MS, become much more powerful when combined with even modest and fast separations offered by TLC (HPTLC).

In the publication III, the first innovative use of laser triangulation – coupled also with the unique DAPPI technique – for the nonplanar surface analysis in ambient mass spectrometry was presented. The automatic adjustment of the vertical distance between the sample and the entrance capillary offers new applications and ways of the ion source operation. In the simplest way, the movement of the stage in the vertical direction can be used for an automated ion source tuning for the optimum position of planar samples. As regards nonplanar samples, the ion source offers analysis of objects with variable height, e.g., pieces or cuts of fruit or vegetable for pesticide screening and analyzing tablets of various size. For this type of sample, the measuring height is automatically adjusted for the object height. The most attractive, but also the most demanding is the surface analysis. The presented ion source offers a new cost-effective alternative beneficially used, for instance, in the rapid screening of product quality. What is more, the measurable sample height is limited only be the type of the used sensor (20 mm for the presented ion source).

Two ambient MS methods for the rapid monitoring of steroid metabolites during pregnancy were studied in the publication IV. Both techniques were found suitable for the task: DAPPI detected C19 and C21 steroid metabolites in the samples, while DESI gave signals for C18, C19, and C21 steroid metabolites. In particular, the progress of pregnancy lead to over an order of magnitude increase for at least ten steroid ion signals analyzed by LLE–DAPPI–HRMS, and a similar increase of at least 11 ions of steroid sulfates or glucuronides and one unidentified ion according to SPE–DESI–HRMS. Both studied methods were found suitable for the monitoring of selected steroid metabolites during pregnancy, but the DESI method is especially attractive due to simpler sample preparation that does not require hydrolysis of analytes, the ease of interpretation of results, and better sensitivity especially for C18 steroids. Moreover, it shows promise for the extremely quick screening of urinary steroids challenging commonly employed methods.

REFERENCES

1. Yamashita, M.; Fenn, J. B. *J. Phys. Chem.* **1984**, *88*, 4451–4459.

2. Syage, J. A.; Evans, M. D.; Hanold, K. A. *Am. Lab.* **2000**, *32*, 24–29.

3. Robb, D. B.; Covey, T. R.; Bruins, A. P. *Anal. Chem.* **2000**, *72*, 3653–3659.

4. Laiko, V. V.; Baldwin, M. A.; Burlingame, A. L. *Anal. Chem.* **2000**, *72*, 652–657.

5. Bothner, B.; Siuzdak, G. *ChemBioChem* **2004**, *5*, 258–260.

6. Takáts, Z.; Wiseman, J. M.; Cologan, B.; Cooks, R. G. *Science* **2004**, *306*, 471–473.

7. Haapala, M.; Pól, J.; Saarela, V.; Arvola, V.; Kotiaho, T.; Ketola, R. A.; Franssila, S.; Kauppila, T. J.; Kostiainen, R. *Anal. Chem.* **2007**, *79*, 7867–7872.

8. Harris, G. A.; Galhena, A. S.; Fernandéz, F. M. *Anal. Chem.* **2011**, *83*, 4508–4538.

9. Laurent, P.; Braekman J. C.; Daloze, D. *Top. Curr. Chem.* **2005**, *240*, 167–229.

10. Cheng, S. Y.; Huang, M. Z.; Shiea, J. *J. Chromatogr. A* **2011**, *1218*, 2700−2711.

11. Nguyen, S. N.; Liyu, A. V.; Chu, R. K.; Anderton, C. R.; Laskin, J. *Anal. Chem.* **2017**, *89*, 1131–1137.

12. Cody, R. B.; Laramee, J. A.; Durst, H. D. *Anal. Chem.* **2005**, *77*, 2297–2302.

13. McEwen, C. N.; McKay, R. G.; Larsen, B. S. *J. Am. Soc. Mass Spectrom.* **2005**, *77*, 7826–7831.

14. Williams, J. P.; Patel, V. J.; Holland, R.; Scrivens, J. H. *Rapid Commun. Mass Spectrom.* **2006**, *20*, 1447–1456.

15. Haddad, R.; Sparrapan, R.; Eberlin, M. N. *Rapid Commun. Mass Spectrom.* **2006**, *20*, 2901–2905.

16. Chen, H.; Venter, A.; Cooks, R. G. *Chem. Commun.* **2006**, *19*, 2042–2044.

17. Huang, M. Z.; Hsu, H. J.; Lee, J. Y.; Jeng, J.; Shiea, J. *J. Proteome Res.* **2006**, *5*, 1107–1116.

18. Sampson, J. S.; Hawkridge, A. M.; Muddiman, D. C. *J. Am. Soc. Mass Spectrom.* **2006**, *17*, 1712–1716.

19. Chen, H.; Yang, S.; Wortmann, A.; Zenobi, R. *Angew. Chem. Int. Ed.* **2007**, *46*, 7591–7594.

20. Ratcliffe, L. V.; Rutten, F. J. M.; Barrett, D. A.; Whitmore, T.; Seymour, D.; Greenwood, C.; Aranda-Gonzalvo, Y.; Robinson, S.; McCoustra, M. *Anal. Chem.* **2007**, *79*, 6094–6101.

21. Sonnenfeld, A.; Tun, T. M.; Zajícková, L.; Kozlov, K. V.; Wagner, H. E.; Behnke, J. F.; Hippler, R. *Plasma Process. Polym.* **2001**, *6*, 237–266.

22. Haddad, R.; Sparrapan, R.; Kotiaho, T.; Eberlin, M. N. *Anal. Chem.* **2008**, *80*, 898–903.

23. Andrade, F. J.; Shelley, J. T.; Wetzel, W. C.; Webb, M. R.; Gamez, G.; Ray, S. J.; Hieftje, G. M. *Anal. Chem.* **2008**, *80*, 2654–2663.

24. Takats, Z.; Nanita, S. C.; Cooks, R. G.; Schlosser, G.; Karoly Vekey, K. *Anal. Chem.* **2003**, *75*, 1514–1523.

25. Cody, R. B. *Anal. Chem.* **2009**, *81*, 1101–1107.

26. Wang, H.; Liu, J.; Cooks, R. G.; Ouyang, Z. *Angew. Chem. Int. Ed.* **2010**, *49*, 877–880.

27. Xu, S.; Zhang, Y.; Xu, L.; Bai, Y.; Liu, H. *Analyst* **2016**, *141*, 5913–5921.

28. Alberici, R. M.; Simas, R. C.; Sanvido, G. B.; Romao, W.; Lalli, P. M.; Benassi, M.; Cunha, I. B. S.; Eberlin, M. N. *Anal. Bioanal. Chem.* **2010**, *398*, 265–294.

29. Ostman, P.; Martilla, S. J.; Kotiaho, T.; Franssila, S.; Kostiainen, R. *Anal. Chem.* **2004**, *76*, 6659–6664.

30. Syage, J. A. *J. Am. Soc. Mass Spectrom.* **2004**, *15*, 1521–1533.

31. Robb, D. B.; Covey, T. R.; Bruins, A. P. *Anal. Chem.* **2000**, *72*, 3653–3659.

32. Luosujarvi, L.; Arvola, V.; Haapala, M.; Pol, J.; Saarela, V.; Franssila, S.; Kotiaho, T.; Kostiainen, R.; Kaupilla, T. J. *Anal. Chem.* **2008**, *80*, 7460–7466.

33. Pasilis, S. P.; Kertesz, V.; Van Berkel, G. J. *Anal. Chem.* **2008**, *80*, 1208–1214.

34. Venter, A.; Sojka, P. E.; Cooks, R. G. Anal. Chem. 2006, 78, 8549-8555.

35. Luosujärvi, L.; Kanerva, S.; Saarela, V.; Franssila, S.; Kostiainen, R.; Kotiaho, T.; Kauppila, T. J. *Rapid Commun. Mass Spectrom*. **2010**, *24*, 1343–1350.

36. Luosujärvi, L.; Laakkonen, U. M.; Kostiainen, R.; Kotiaho, T.; Kauppila, T. J. *Rapid Commun. Mass Spectrom.* **2009**, *23*, 1401–1404.

37. Kauppila, T. J.; Flink, A.; Laakkonen, U. M.; Aalberg, L.; Ketola, R. A. *Drug Test. Anal.* **2013**, *5*, 186–190.

38. Pól, J.; Vidová, V.; Kruppa, G.; Kobliha, V.; Novák, P.; Lemr, K.; Kotiaho, T.; Kostiainen, R.; Havlíček, V.; Volný, M. *Anal. Chem.* **2009**, *81*, 8479–8487.
39. Ifa, D. R.; Rusine, A. L.; Cooks, R. G. *Rapid Commun. Mass Spectrom.* **2008**, *22*, 503–510.
40. Cooks, R. G.; Ouyang, Z.; Takats, Z.; Wiseman, J. M. *Science* **2006**, *311*, 1566–1570.
41. Costa, A. B.; Cooks, R. G. *Chem. Phys. Lett.* **2008**, *464*, 1–8.
42. Shin, Y. S.; Drolet, B.; Mayer, R.; Dolence, K.; Basile, F. *Anal. Chem.* **2007**, *79*, 3514–3518.
43. Volný, M.; Venter, A.; Smith, S. A.; Pazzi, M.; Cooks, R. G. *Analyst* **2008**, *133*, 525–531.
44. Weston, D. J.; Bateman, R.; Wilson, I. D.; Wood, T. R.; Creaser, C. S. *Anal. Chem.* **2005**, *77*, 7572–7580.
45. Cotte-Rodriguez, I.; Hernandez-Soto, H.; Chen, H.; Cooks, R. G. *Anal. Chem.* **2008**, *80*, 1512–1519.
46. Ifa, D. R.; Wiseman, J. M.; Song, Q.; Cooks, R. G. *Int. J. Mass Spectrom.* **2007**, *259*, 8–15.
47. Ifa, D. R.; Gumaelius, L. M.; Eberlin, L. S.; Manicke, N. E.; Cooks, R. G. *Analyst* **2007**, *132*, 461–467.
48. Fernandez, F. M.; Cody, R. B.; Green, M. D.; Hampton, C. Y.; McGready, R.; Sengaloundeth, S.; White, N. J.; Newton, P. N. *ChemMedChem* **2006**, *1*, 702–705.
49. Kauppila, T. J.; Talaty, N.; Salo, P. K.; Kotiaho, T.; Kostiainen, R.; Cooks, R. G. *Rapid Commun. Mass Spectrom.* **2006**, *20*, 2143–2150.
50. Yang, S.; Han, J.; Huan, Y.; Cui, Y.; Zhang, X.; Chen, H.; Gu, H. *Anal. Chem.* **2009**, *81*, 6070–6079.
51. Pasilis, S. P.; Kertesz, V.; Van Berkel, G. J.; Schulz, M.; Schorcht, S. *J. Mass Spectrom.* **2008**, *43*, 1627–1635.
52. Valentine, S. J.; Plasencia, M. D.; Liu, X.; Krishnan, M.; Naylor, S.; Udseth, H. R.; Smith, R. D.; Clemmer, D. E. *J. Proteome Res.* **2006**, *5*, 2977–2984.
53. Chen, H.; Pan, Z.; Talaty, N.; Raftery, D.; Cooks, R. G. *Rapid Commun. Mass Spectrom.* **2006**, *20*, 1577–1584.
54. Van Berkel, G. J.; Ford, M. J.; Deibel, M. A. *Anal. Chem.* **2005**, *77*, 1207–1215.

55. Jackson, A. U.; Tata, A.; Wu, C.; Perry, R. H.; Haas, G.; West, L.; Cooks, R. G. *Analyst* **2009**, *134*, 867–874.
56. Talaty, N.; Takats, Z.; Cooks, R. G. *Analyst* **2005**, *130*, 1624–1633.
57. Song, Y.; Talaty, N.; Datsenko, K.; Wanner, B. L.; Cooks, R. G. *Analyst* **2009**, *134*, 838–841.
58. Li, M.; Chen, H.; Yang, X.; Chen, J.; Li, C. *Atmos. Environ.* **2009**, *43*, 2717–2720.
59. Jackson, A. T.; Williams, J. P.; Scrivens, J. H. *Rapid Commun. Mass Spectrom.* **2006**, *20*, 2717–2727.
60. Kuldová, J.; Hrdý, I.; Svatoš, A. *J. Chem. Ecol.* **1999**, *25*, 657–662.
61. Šubčíková, L.; Hoskovec, M.; Vrkoslav, V.; Čmelíková, T.; Háková, E.; Míková, R.; Coufal, P.; Doležal, A.; Plavka, R.; Cvačka, J. *J. Chromatogr. A* **2015**, *1378*, 8−18.
62. Zhang, H.; Henion, J. *Anal. Chem.* **1999**, *71*, 3955–3964.
63. Leinonen, A.; Kuuranne, T.; Kotiaho, T.; Kostiainen, R. *Steroids* **2004**, *69*, 101–109.
64. Ahonen, L. L.; Haapala, M.; Saarela, V.; Franssila, S.; Kotiaho, T.; Kostiainen, R. *Rapid Commun. Mass Spectrom.* **2010**, *24*, 958–964.
65. Saarela, V.; Haapala, M.; Kostiainen, R.; Kotiaho, T.; Franssila, S. *Lab Chip* **2007**, *7*, 644–646.
66. Christie, W. W. *Lipid Analysis*, 3rd ed.; The Oily Press: Bridgwater, 2003.
67. Nes, W. D. *Chem. Rev.* **2011**, *111*, 6423−6451.
68. Lísa, M.; Holčapek, M. *J. Chromatogr. A* **2008**, *1198−1199*, 115−130.
69. Vrkoslav, V.; Urbanová, K.; Cvačka, J. *J. Chromatogr. A* **2010**, *1217*, 4184−4194.
70. Buchgraber, M.; Ulberth, F.; Emons, H.; Anklam, E. *Eur. J. Lipid Sci. Technol.* **2004**, *106*, 621−648.
71. Rhodes, S. H.; Netting, A. G. *J. Chromatogr.* **1988**, *448*, 135−143.
72. Cai, Y.; Kingery, D.; McConnell, O.; Bach II, A. C. *Rapid Commun. Mass Spectrom.* **2005**, *19*, 1717–1724.
73. Yamamoto, A.; Kakutani, N.; Yamamoto, K.; Kamiura, T.; Miyakoda, H. *Environ. Sci. Technol.* **2006**, *40*, 4132–4137.
74. Greig, M. J.; Bolaños, B.; Quenzer, T.; Bylund, J. M. R. *Rapid Commun. Mass Spectrom.* **2003**, *17*, 2763–2768.

75. Ceglarek, U.; Werner, M.; Kortz, L.; Körner, A.; Kiess, W.; Thiery, J.; Kratzsch, J. *J. Steroid Biochem. Mol. Biol.* **2010**, *121*, 505–512.
76. Chang, K.; Zhang, L. *Reprod. Sci.* **2008**, *15*, 336–348.
77. Hill, M.; Pařízek, A.; Cibula, D.; Kancheva, R.; Jirásek, J. E.; Jirkovská, M.; Velíková, M.; Kubátová, J.; Klímková, M.; Pašková, A.; Žižka, Z.; Kancheva, L.; Kazihnitková, H.; Zamrazilová, L.; Stárka, L. *J. Steroid Biochem. Mol. Biol.* **2010**, *122*, 114–132.
78. O'Leary, P.; Boyne, P.; Flett, P.; Beilby, J.; James, I. *Clin. Chem.* **1991**, *37*, 667–672.
79. Soldin, O. P.; Guo, T.; Weiderpass, E.; Tractenberg, R. E.; Hilakivi-Clarke, L.; Soldin, S. J. *Fertil. Steril.* **2005**, *84*, 701–710.
80. Jäntti, S. E.; Hartonen, M.; Hilvo, M.; Nygren, H.; Hyötyläinen, T.; Ketola, R. A.; Kostiainen, R. *Anal. Chim. Acta* **2013**, *802*, 56–66.

APPENDIX – REPRINTED ORIGINAL PUBLICATIONS